The Astrophysical Journal (in press)

Evolutionary Properties of Helium-Rich, Degenerate Dwarfs in Binaries Containing Compact Companions

Lorne A. Nelson[1], Ernest Dubeau, and Keith A. MacCannell

Physics Department, Bishop's University
Lennoxville, Quebec Canada J1M 1Z7

ABSTRACT

The evolution of binaries containing low-mass donors ($\leq 2M_{\odot}$) and degenerate accretors (i.e., white dwarfs [$0.7M_{\odot}$] or neutron stars [$1.4M_{\odot}$]) is systematically investigated over a wide expanse of parameter space. The donors are assumed to have metallicities in the range of $0.0001 \leq Z \leq 0.02$ and could either be unevolved (ZAMS) or could be ascending the red giant branch (RGB) at the onset of mass transfer (corresponding to $5 \lesssim P_{orb}(\mathrm{hr}) \lesssim 2 \times 10^3$). Each evolutionary track forms part of a very detailed grid of nearly 200 sequences each corresponding to a different set of initial conditions. During the initial phases of their evolution, the systems resemble either Low Mass X-Ray Binaries (LMXB's) or Cataclysmic Variables (CV's). However, as has been pointed out by several authors (e.g., Podsiadlowski et al. 2002), the evolutionary tracks can exhibit a wide variety of behaviors and outcomes. We focus on systems that evolve to produce helium-rich degenerate dwarfs (HeDD's) that are either detached or still losing mass after a Hubble time. Of the systems that avoid dynamical instability, some evolve to ultrashort P_{orb}'s (< 60 minutes) while others that lie above the bifurcation limit (which we show to be quite sensitive to the assumed metallicity) produce wide binary millisecond pulsars (BMSP's) containing HeDD companions that have P_{orb}'s of $\lesssim 2 \times 10^4$ hours.

We also show that the mass and composition of the envelopes of HeDD's that are about to descend the cooling branch are particularly sensitive to the input physics and the initial conditions, and this in turn dictates whether they experience extremely vigorous hydrogen shell flashes. The final structure of the envelopes plays a critical role in determining the cooling times of HeDD's. Our

[1]email: lnelson@ubishops.ca

computed values of the envelope mass, m_{env} (corresponding to the mass of those layers below the surface containing some hydrogen), typically lie in the middle of the range of values quoted previously. At late ages we find that the envelope masses have a dependence on the final donor mass (m_f) and metallicity (Z) that can be expressed as $m_{env} \propto m_f^{-2.8}\ Z^{-0.2}$. Furthermore, for systems that do not evolve too close to the bifurcation limit, we find that the final orbital period is given by $P_{orb,f}(\mathrm{hr}) = 2.5\ Z^{0.3}\ 10^{10.7(m_f/M_\odot)}$. Finally we use our results to comment on the properties of the optical companions to binary millisecond pulsars and compare their inferred ages with the spin-down times of the pulsars. The structure of young HeDD's should be particularly useful as starting models for more sophisticated cooling calculations that take into account important long-term physical processes and thus we are making our models available for retrieval.

Subject headings: − binaries: close − low-mass x-ray binaries − pulsars: millisecond − stars: evolution − stars: mass loss − stars: low mass − stars: hydrogen-depleted

1. Introduction

Many Cataclysmic Variables (CV's) and Low Mass X-Ray Binary systems (LMXB's) are believed to be interacting binaries wherein a low-mass donor transfers matter to a compact object (a white dwarf or neutron star, respectively). Podsiadlowski et al. (2002; PRP) showed that many of the donors in LMXB's may have descended from intermediate-mass stars[2]. According to the standard model, the donor star (secondary) overflows its Roche lobe (RLOF) and matter is transferred (for non-magnetic systems) via an accretion disk to the surface of the compact object (see, e.g., Warner 1995, and references therein). The first generation of self-consistent theoretical models describing the evolution of low-mass systems assumed that the donor was a ZAMS star at the onset of mass transfer (see, e.g., Paczyński & Sienkiewicz 1981; Rappaport, Joss, & Webbink 1982 [RJW]; Spruit & Ritter 1983; Rappaport, Verbunt, & Joss 1984 [RVJ]; Hameury et al. 1988, D'Antona, Mazzitelli, & Ritter 1989). Later models examined the evolution of interacting binaries containing compact objects under the assumption that the donor was in various states of advanced chemical evolution prior to the onset of mass transfer (see, e.g., Tutukov et al. 1985; Iben & Tutukov 1986 [IT]; Pylyser & Savonije 1988 [PS], 1989; Schenker, Kolb & Ritter 1998;

[2]Since the accretors in LMXB's (i.e., neutron stars) have higher masses (on average) than those in CV's (i.e., degenerate dwarfs), they can accommodate higher mass donors without suffering a dynamical instability.

Nelson, MacCannell & Davis 2001; PRP). Among other things, they found that sufficiently evolved donors that did not become giants could evolve to ultrashort orbital periods (< 1 hr) while those that were sufficiently evolved to become (sub)giants would ultimately produce detached systems containing cooling, HeDD's in orbit with their compact companions. For the case of neutron-star accretors, the latter systems end up as wide (nearly circular), low-mass binary millisecond pulsars [LMBP's] (see, for example, Alpar et al. 1982, Joss & Rappaport 1983, and Bhattacharya & van den Heuvel 1991 for a review). The pulsars in these systems are often referred to as "recycled" because they have been spun up by accretion torques. The formation and/or cooling of HeDD's in LMBP's have been studied by Alberts et al. 1996, Althaus & Benvenuto 1997, Benvenuto & Althaus 1998 [BA], Hansen & Phinney 1998a,b [HPa,b], Driebe et al. 1998 [DSBH], Tauris & Savonije (1999) [TS], Saran, Ergma, & Gerskevits-Antipova 2000 [SEG], Nelson & Davis 2000 [ND], Althaus, Serenelli & Benvenuto 2001 [ASB], and PRP. By accurately determining the cooling times of the HeDD's (and thus the age of the pulsar after it has 'turned on'), it may be possible to comment on the spin-down evolution of the pulsars (see HPb). In this paper we analyze the properties of HeDD's that are likely to be found in LMBP's for a very wide range of metallicities (Z) and masses.

The evolutionary pathways leading to the formation of binaries containing compact objects is becoming better understood and many of the salient features of these systems (e.g., the observed number of systems as a function of the orbital period) have been explained using population synthesis techniques (see, for example, Howell, Nelson & Rappaport 2001 [HNR]; Willems & Kolb 2002, Pfahl, Rappaport & Podsiadlowski 2003, and references therein). However, there are still many unanswered questions concerning the formation of these systems, especially those for which neutron stars or black holes are the compact companions. With regard to the formation of CV's it is generally accepted that the compact companion (i.e., white dwarf) was formed as a result of the "spiral-in" of the companion (secondary) during a common envelope phase of evolution (see, e.g., Taam, Bodenheimer, & Ostriker 1978; Meyer & Meyer-Hofmeister 1979; Livio & Soker 1988; Webbink 1992; Kalogera & Webbink 1998; Dewi & Taurus 2000). After the ejection of the common envelope (CE), the separation between the secondary and the newly formed white dwarf is determined by energetic considerations. Unfortunately the physics associated with the ejection event is very complicated but it is expected that (assuming a merger does not occur) the separation of the two stars would be greatly reduced. If the components are sufficiently close after the CE phase, magnetic stellar wind (MSW) braking may be able to bring the secondary (now the donor) into contact with its Roche lobe while it is still a ZAMS star. However, depending on assumptions concerning the efficiency of orbital energy conversion and the effectiveness of MSW braking, the post CE separation may be so wide that MSW's are unable to bring

about contact. If this is the case, then barring some other form of orbital angular momentum dissipation, the secondary will only start to lose mass if it expands as a result of nuclear evolution. The detailed evolution and ultimate fate of the binary system depends on the magnitudes of the relevant physical timescales (e.g., the mass-loss timescale [$\tau_{\dot{m}}$]; the thermal timescale of the donor [τ_{KH} or τ_{env}]; and, the nuclear timescale [τ_{nuc}]). Donors for which $\tau_{nuc} \ll \tau_{\dot{m}}$ have sufficiently short nuclear timescales that they can become giants before losing too much mass. These latter systems can evolve to very long orbital periods (up to hundreds of days) before the donors detach from their Roche lobes leaving behind a helium degenerate dwarf [HeDD] in orbit with a recycled pulsar (e.g., PSR1855+09). For systems for which $\tau_{nuc} \gg \tau_{\dot{m}}$, the evolution is governed largely by orbital angular momentum losses due to gravitational radiation, MSW braking, and systemic mass loss. The delineation of these two regimes is marked by the bifurcation limit (see, e.g., PS).

Binaries below the bifurcation limit typically evolve from orbital periods on the order of 10 hours to a minimum orbital period (on the order of one hour) and then back to increasing orbital periods. The theoretical evolution of CV's has been quite well studied (see, e.g., Warner 1995, and HNR for more recent references). If the donor has not had time to evolve chemically once it commences mass transfer (i.e., it is approximately homogeneous) then the theoretical models show that it will evolve from long orbital periods ($\sim$ 6 hours for a $1M_{\odot}$ donor) to short orbital periods ($\sim$ 1.2 hours) and then back up to periods of $\sim$ 3 hours given a sufficient amount of time. If the magnitude of magnetic stellar braking is greatly attenuated when the internal structure of the donor becomes fully convective then it is possible for the donor to shrink beneath its Roche lobe with the concomitant cessation of mass transfer (see, e.g., RVJ). Eventually the donor will be brought back into contact with its Roche lobe as the result of gravitational radiation losses and recommence mass transfer. This scenario is the most plausible explanation of the so-called 2 - 3 hour "period gap" that has been observed for CV systems (Kolb, King, & Ritter 1998). Some CV's and LMXB's have orbital periods much smaller than the predicted theoretical minimum orbital period of approximately 80 minutes and it is thought that some of these systems can be explained by donors that are hydrogen depleted (see, e.g., Tutukov et al. 1985; Nelson, Rappaport, & Joss 1986 [NRJ]; Ergma, Sarna & Antipova 1998; PRP; Nelson & Rappaport 2003 [NR]; Podsiadlowski, Han & Rappaport 2003). These include the CV's such as AM CVn (17.1 min) and LMXB's such as 4U 1820-30 (11.4 min). Five accreting millisecond pulsars have also been recently discovered and three have ultrashort orbital periods: XTE J1751-305 (42.4 min), XTE J0929-314 (43.6 min), XTE J1814-338 (43.6 min), and XTE J1807-294 ($\lesssim$ 40 min). For some of these systems we would expect that the donor could initially have been a low-mass star ($\sim 1M_{\odot}$), that would necessarily be somewhat evolved (e.g., near TAMS)

at the onset of mass transfer[3]. Higher mass donors would not have to be as evolved but would have to undergo significant nuclear evolution during the mass transfer phase in order to achieve the necessary degree of hydrogen depletion (see PRP). [We note that for the case of CV's with $\sim 0.7 M_{\odot}$ DD accretors that the initial mass of the donor cannot be much greater than $\sim 1.5 M_{\odot}$ since the relatively high mass ratio $q \equiv M_2/M_1$ would likely result in a dynamical instability and the merger of the system.]

In this paper we undertake a detailed exploration of interacting binary systems consisting of compact objects and low-mass donors that are (arbitrarily) evolved at the onset of mass transfer (either approaching TAMS, or ascending the RGB). A wide expanse of parameter space has been explored and is complementary to previous work (e.g., PS, HP, DSBH, SEG, ASB, and PRP). While only one mode of systemic angular momentum loss is considered, models covering the widest range of metallicities and initial chemical profiles are carefully calculated. The overall computational effort required more than 10^{16} floating point operations and generated more than one terabyte of data ($\sim$ 200 tracks were calculated). Particular attention is paid to the formation and evolution of HeDD's that are likely to be found as companions to pulsars in LMBP's. The properties of these objects are very sensitive to the assumed input physics and initial conditions. Some HeDD's experience vigorous hydrogen shell flashes (due to unstable CNO burning in a thin H-rich layer near their surfaces) while others experience mild thermal instabilities. The composition and mass (m_{env}) of the envelopes, the presence of residual nuclear burning and possible shell flashes can have a significant effect on the inferred cooling times of the HeDD companions (and thus on the inferred age of pulsar itself). Previous calculations of the cooling properties of HeDD's show many similarities (see, e.g., HP, DSBH, SEG, ASB, PRP), but there are also many significant differences with the present work. We examine them in detail and show that the dependence of some of the central properties (e.g., m_{env}) can be quantified in terms of m_f and Z.

The basic results of these computations are available for retrieval on the server **physics.ubishops.ca/evolution**. Our library of calculations also serve two other purposes. First, they form part of the library of tracks that constitute the MULTIGRID project which will ultimately archive more than 5000 evolutionary sequences (Nelson & Dubeau 2004a). The initial conditions for these sequences will be much more finely spaced (in parameter space), especially for binaries near the bifurcation limit. This library should make it possible to carry out binary population syntheses more efficiently (i.e., using interpolation techniques on existing sequences). Second, the results presented in this paper will also serve as a

[3]It is important to note that other evolutionary pathways wherein HeDD's or hybrid HeCO DD's lose mass to their neutron star companion could easily be invoked to explain the ultrashort orbital periods.

"calibration standard" for a new 'fast-code' that we are developing to carry out on-the-fly binary evolution calculations (Nelson & Rappaport 2004). Such fast binary evolution codes (typically requiring ≈ 1 CPU minute per track) would be of great use to researchers involved in binary population synthesis studies, and in particular for the MODEST group that is working on a comprehensive program to study the evolution of globular clusters. The main advantage of using the fast-code is that individual evolutionary tracks can be calculated (as opposed to interpolations), thus giving researchers working on binary population syntheses more flexibility (e.g., angular momentum dissipation can be arbitrarily adjusted).

In §2 of this paper we describe the input physics that was used to carry out the computations. We also describe the calculation of the evolutionary sequences in detail as well as the range of initial conditions that was investigated. In §3 we present the results of the computations including the evolution of donors through the HR diagram and the evolution of their observable properties. We also discuss the effects of the input physics on the bifurcation limit and explore some of the issues associated with hydrogen shell flashes and show how the dependence of certain important properties can be quantified. In §4 we look at specific applications to observed binary systems. Our conclusions and plans for future work are summarized in the final section.

2. Methodology

All of the binary evolution calculations described in this paper were carried out using the Lagrangian-based Henyey method. The basic code has been described in several papers (see, e.g., Nelson, Chau & Rosenblum 1985; Dorman, Nelson & Chau 1989) and has been extensively tested. In the version of the code that was used to produce the calculations presented in this paper, we took the donor star to be spherical and used the volume-averaged radius formula of Eggleton (1983) to relate to the orbital separation A and volume-averaged radius R_2 of the donor (secondary) star. In terms of the mass ratio q ($\equiv M_2/M_1$), this formula can be expressed as

$$\frac{R_2}{A} = \frac{0.49q^{2/3}}{0.6q^{2/3} + \ln(1+q^{1/3})} \ . \tag{1}$$

For small values of q ($\lesssim 0.1$) this approximation for R_2/A is more accurate than that derived using the method of Chan and Chau (1979; the difference in the two estimates is ~ 2 %). The most important refinements in the code are due to improvements in the input physics, particularly the opacities. We use the OPAL radiative opacities (Iglesias & Rogers, 1996; Grevesse 1993 composition) in conjunction with the low-temperature opacities of Alexander & Ferguson (1994), and the Hubbard & Lampe (1969) conductive opacities. Evolutionary

calculations such as the ones presented in this paper require that the independent variables (e.g., T, ρ, and chemical composition) describing the properties of the donors span many orders of magnitude. Great care has been taken to ensure that each of these opacities blends smoothly across their respective boundaries of validity. Our treatment also enforces continuity of the respective first-order partial derivatives.

The equation of state (EOS) that is used is a combination of an analytic EOS for arbitrary mixtures of hydrogen, helium, and heavier elements that was matched to the Magni & Mazzitelli (1979) EOS for helium. The analytic EOS includes the effects of molecular hydrogen formation, radiation pressure, arbitrarily relativistic electron degeneracy, and an approximate treatment of pressure ionization. The effects of plasma neutrino cooling due to the method of Itoh et al. (1990) are also included in the computations. Since pressure ionization and Coulombic (plasma) coupling can be extremely important considerations in determining the detailed structure of the interiors of low-temperature (and low-mass) stars, we generally terminated our evolutionary sequences once the mass of the donor has dropped to $\lesssim 0.1 M_{\odot}$. We find that the treatment of pressure ionization can have a very significant effect on the computed properties of all low-mass models ($\lesssim 0.2 M_{\odot}$). This issue is addressed in more detail by NR who used the Saumon, Chabrier & Van Horn (1995) EOS to evolve very low-mass, cold, donors.

Special attention is paid to ensuring high accuracy in the calculation of the structure of the outer layers (i.e., the envelope). These outer layers primarily determine the cooling times of the helium-rich remnants. The fitting point that delineates the interior structure (solved by a relaxation technique) from the envelope (solved by a Newton-Raphson integration under the assumption of a constant luminosity) was determined adaptively; in some cases, the fractional mass of the envelope is as small as 10^{-6} ($= 1 - m_{env}/M_{star}$). While this increases the number of shells needed to describe the interior structure, it decreases the inaccuracy that is caused by the assumption that the 'gravothermal' contribution to the luminosity (i.e., L_g) in the envelope is zero. Moreover, hydrogen shell flashes can occur very close to the surface (within the outer 1% of the mass of the star) and consequently many (thin) shells above the burning region are needed to ensure high accuracy. We also require that only a small amount of mass be removed from the donor star in each time step. In particular, we ensure that ΔM_2 (i.e., the mass stripped from the donor in a given time step Δt) is approximately of the same order of magnitude of the mass in the first few shells below the envelope. For this reason ΔM_2 was typically less than $10^{-5} M_{\odot}$ per model (and much smaller near the cessation of mass transfer). Consequently each evolutionary track typically consisted of more than 10^5 models and sometimes surpassed 10^6 models. For particularly rapid phases of evolution (i.e., hydrogen shell flashes) the evolutionary timesteps sometimes had to be reduced to values on

the order of hours. The thermal relaxation time of a shell of mass m_{sh} may be defined as

$$\tau_{sh} \simeq \frac{GM_2\ m_{sh}}{R_2\ L_2}\ , \tag{2}$$

where M_2, R_2, and L_2 are the mass, radius, and luminosity of the donor, respectively. It is important to note that some of the outer shells have extremely short relaxation times, and thus by choosing inappropriately large timesteps, the growth of thermal instabilities could be numerically suppressed or inhibited. This in turn may have a significant effect on the long-term evolution of the remnant donor star and the final mass and composition of its envelope.

The parameter space needed to fully investigate the evolution of this type of binary system is inherently five dimensional. The vector of parameter space contains the following elements: (i) the initial mass of the donor ($M_{2,o}$); (ii) the initial mass of the accretor ($M_{1,o}$); (iii) the initial chemical profile of the interior of the donor star; (iv) the metallicity of the donor (Z); and, (v) the mode of angular momentum loss that drives mass transfer and the degree to which systemic mass loss occurs. The resolution of the grid of models is simply constrained by the available computing power. We calculate approximately 200 evolutionary tracks corresponding to initial donor masses of $M_{2,o} = 1$, 1.5, and $2M_{\odot}$, while the masses of the accretors are taken to be $M_{1,o} = 0.7$ (i.e, a mass appropriate for a degenerate dwarf [DD] accretor in a CV) or $1.4M_{\odot}$ (i.e, a mass appropriate for a neutron star in an LMXB). The initial chemical profile of the donor is parameterized in terms of either $X_{c,o}$ or $m_{c,o}$. The initial central hydrogen mass fractions (at the onset of mass transfer) are taken to be in the range of $0 \leq X_{c,o} \leq 0.71$. For the cases corresponding to zero central hydrogen, the helium core masses are in the range of $0 \leq (m_{c,o}/M_{\odot}) \leq 0.40$. The initial hydrogen abundance (by mass) on the ZAMS is taken to be equal to 0.71, the ratio of the mixing length to the pressure scale-height ratio (l/H_p) is set equal to 1.5, and the metallicity is chosen to be representative of Population I and II stars. Specifically we calculate models of donors whose metallicity is $Z = 0.0001$, 0.004, and 0.02. The number of shells needed to adequately describe the interior structure varies enormously depending on the evolutionary state of the donor. For example, when the donor is not very chemically evolved or when it is in a cooling stage (having detached from its Roche lobe), then only a couple hundred shells sufficed. However, during complicated and/or rapid phases of the evolution (e.g., near helium flash) sometimes more than 3000 shells are needed. For the sake of accuracy, we do not use "shell shifting" methods to approximate thin-shell H-burning.

It is assumed that gravitational radiation and MSW braking are responsible for orbital angular momentum losses. Angular momentum losses due to gravitational radiation are calculated using the Landau-Lifshitz (1962) radiation-reaction formula. This can be expressed

as

$$\frac{\dot{J}_{GR}}{J} = -8.3 \times 10^{-10} \left[\frac{m_1 m_2 m_T}{a^4}\right] \quad \mathrm{yr}^{-1} \ , \tag{3}$$

where the variables m_1, m_2, and m_T $(= m_1 + m_2)$ are given in solar units, and a is the orbital separation in units of $R_\odot$. We use the RVJ parameterization of the Verbunt-Zwaan (1981) braking law (i.e., $\dot{J}_{MB} \propto R_2^\gamma$ where γ is a dimensionless number). This can be expressed as

$$\frac{\dot{J}_{MB}}{J} = -2.3 \times 10^{-6} f_{MB} \left[\frac{m_T^2 \ r^\gamma}{m_1 \ a^5}\right] \quad \mathrm{yr}^{-1} \ , \tag{4}$$

where $r = R_2/R_\odot$ and f_{MB} is a dimensionless function that takes into account the moment of inertia of the donor (its magnitude is of order 0.1). For the present investigation, we set $\gamma = 3$ since this value approximately reproduces the observed period gap in the distribution of CV orbital periods. The exact value of the radius of gyration of the donor star is calculated using the computed internal structure of the donor. We do not, however, interrupt magnetic braking if the interior structure of the donor becomes completely convective (for a discussion of this issue see HNR, and references therein). We note that chemically evolved donors will temporarily stop transferring mass at relatively shorter orbital periods (i.e., less than three hours) and that the width of the gap will also be smaller (see NR for more details). Finally we caution that the magnitude of the magnetic braking torques acting on these donors are not very well known.

Mass transfer is assumed to be completely non-conservative. We thus set the mass-capture fraction (i.e., $\beta \equiv \dot{M}_1/|\dot{M}_2|$) equal to zero, and assume that the matter lost from the system is lost rapidly and isotropically and that it carries away a specific angular momentum equal to that of the compact accretor (i.e., fast Jeans' mode). We note that this assumption is probably very well warranted in the case of CV's during phases of evolution when the mass transfer rates are $\lesssim 5 \times 10^{-9} M_\odot$/yr (see, e.g., Prialnik & Kovetz 1995). At this rate, the matter accreted onto the surface of the degenerate dwarf does not experience steady burning but rather undergoes a series of thermonuclear explosions (i.e., nova events). It is even possible that the DD is eroded during these events (i.e., $\beta < 0$). However, during certain phases of evolution (e.g., thermal timescale mass transfer) it may be possible for the mass capture fraction to be significantly greater than zero ($0 < \beta < 1$). With regard to neutron star companions (in LMXB's and related systems), the situation is much less clear. Systemic mass loss may occur due to inefficient accretion which could be caused by a wind emanating from the atmosphere of the disk due to high radiation pressures or could be the result of relativistic jets. A theoretical study of the evolution of LMXB's by Tauris & Savonije (1999) led them to conclude that a substantial fraction of material is ejected even when the neutron stars are accreting at sub-Eddington levels (they suggest disk instabilities or the propellor

effect as the cause). Based on observational studies of pulsars in all types of binary systems (e.g., Joss & Rappaport 1976; Thorsett & Chakrabarty 1999) we see that their masses are fairly tightly clustered in the range of $\sim 1.3 - 1.8 M_{\odot}$. We would expect millisecond pulsars ($P < 10$ms) to be more massive than they were at birth (accretion torques having spun up the pulsar). While there is some statistical evidence to support this claim, the most precisely determined millisecond pulsar masses are $1.58 \pm 0.18 M_{\odot}$ for PSR J0437+4715 (van Straiten et al. 2001) and $1.57^{+0.12 M_{\odot}}_{-0.11 M_{\odot}}$ for PSR B1855+09 (Nice et al. 2003). This would certainly seem to imply that accretion is inefficient (i.e., $\beta < 1$) and may even be consistent with ~ 0, but we caution that its value is highly uncertain. We adopt $\beta = 0$ as a limiting case but also recognize that it needs to be somewhat larger if the neutron star accretors are to be spun up to millisecond periods (they probably need to accrete $\sim 0.1 M_{\odot}$). For the purposes of comparison, we have calculated the evolution of a large number of tracks under the constraint of purely conservative mass transfer (i.e., $\beta = 1$). We show that for most cases the evolution of the donor star is not greatly affected by this constraint (see §3.1.2 for detailed information).

We have not included the effects of X-ray irradiation on the donor. Some previous calculations have suggested that the effects are small in LMXB's due to absorption by the accretion disk (and possibly a self-excited wind surrounding the disk). Unfortunately the overall importance irradiation in CV's and LMXB's is not well understood. The magnitude of the mass-loss rate due to stellar winds emanating from the donor is also subject to large uncertainties. The most widely used formula is that due to Reimers (1975) but is largely empirical and is best suited for stars ascending (but not near the tip of) the AGB. These issues are discussed in much greater detail by Willson (2000). The effects of winds on the formation and evolution of LMBP's are discussed in §3.3.

3. Evolutionary Results

3.1. Overview

Depending on the initial separation (A) of the binary components after the CE phase of evolution and on the effectiveness of magnetic braking, the differences in the degree of nuclear evolution that has occurred in the donor at the onset of mass loss can be substantial. For example, if the accretor and donor are relatively close to each other after the binary has been formed (or magnetic braking is highly efficient in establishing contact), the donor will not have had much time to evolve before filling its (critical) Roche lobe and thus its value of X_c will be ~ 0.7 when mass transfer first occurs. If the binary is formed with a relatively wide separation, the donor may become a giant (with a large core mass) by the time that

it fills its Roche lobe. Thus the initial chemical profile of the donor (at the onset of mass transfer) is correlated with the orbital separation at the end of the CE phase.

In order to investigate the effects of different initial states (i.e., chemical profiles of the donor) on the evolution of these interacting binary systems, we allow single stars to evolve from the ZAMS to the tip of the red giant branch (i.e., just before the ignition of helium burning). The donor is then brought into contact with its Roche lobe at various points during its chemical evolution (parameterized in terms of X_c and m_c). For donor stars without cores at the onset of mass transfer, our evolutionary tracks are typically calculated for intervals of 0.10 in X_c, and in increments of $0.05M_\odot$ in m_c for donors that have developed cores. The initial orbital periods range from ~ 5 to more than 2000 hours. Since many of the tracks are qualitatively similar, we will not present all of the results but will instead discuss the salient features associated with the metallicity dependence, initial chemical profiles, and the correlation between the final properties (e.g., P_{orb}) and the initial ones. Detailed numerical information for many of the sequences can be found in Tables 1 and 2. In Table 2 the properties of the donor stars are compared for a fixed luminosity of $\log(L/L_\odot) = -1.5$.

In Figures 1-3 we present the evolutionary tracks of $1M_\odot$ donors in the HR diagram for $Z = 0.02$, 0.004, and 0.0001, respectively. The tracks of donors whose initial mass is $1.5M_\odot$ are shown in Figures 4-6 for the same respective metallicities. In both figures the mass of the accretor is $1.4M_\odot$. The most striking features of these figures are: (i) the very distinct bifurcation in the evolutionary tracks (above the limit donors ascend the RGB and produce DD remnants while below the limit donors evolve to ever decreasing luminosities); and, (ii) the occurrence of vigorous hydrogen shell flashes while the donors are about to descend the cooling branch (in the figures, shell-flash tracks are not explicitly shown but begin and end between the dotted lines; see §3.2 for more information). Both of these features have been noted previously in several papers and will be discussed in more detail.

According to Figure 1 we see that donors having initial values of $X_c = 0$, 0.1, and 0.3 ($X_c = 0$ being equivalent to $M_c = 0$) exhibit very different evolutionary behaviors compared to donors that have developed helium cores. The dividing line between these two types of evolution is known as the bifurcation limit. Below the limit the donors lose mass sufficiently rapidly that they never develop a core and thus evolve towards increasingly lower luminosities and effective temperatures. Furthermore, if the mass-transfer timescale is longer than the thermal timescale, the donor will remain in approximate thermal equilibrium and will evolve down the main sequence as its mass is reduced. Below the H-burning limit ($\sim 0.08M_\odot$), the donor begins to evolve towards the degenerate branch. During the early phases of mass transfer its radius continuously decreases leading to a decrease in P_{orb} (see, also Figures 8 & 9). This trend changes when the donor masses are $\lesssim 0.1M_\odot$ and electron degeneracy

dominates the EOS. For unevolved donors ($Z = 0.02$) a minimum orbital period of ~ 1.2 hours is attained (see RJW); the minimum P_{orb} can be much smaller if the donor is more evolved and thus more H-deficient (see, e.g., NR and references therein). As can be seen in Figure 8, the initial values of P_{orb} that lead to evolution below the bifurcation limit are $\lesssim 20$ hours for a solar metallicity (the values are somewhat smaller for lower-mass donors).

For larger core masses ($\geq 0.05 M_{\odot}$; $Z = 0.02$), $\tau_{nuc} << \tau_{\dot{m}}$ thus making it possible for the donors to evolve through the subgiant phase and form helium cores. For many of these donors, their luminosities increase by more than an order of magnitude while simultaneously losing more than one-half of their mass. The H-burning shell continues to burn outwards thereby increasing the mass of the core. As is well-known, the properties of red giants are dictated primarily by their core masses (m_c) and not by the mass of the stars themselves or by the mass-transfer rate, $\dot{M}_2$ (see, e.g., Kippenhahn & Weigert 1990). A number of authors have used this result in the context of interacting binary evolution to show how wide LMXB's evolve and to determine the relationship between the orbital period and core mass (see, e.g., Webbink, Rappaport, & Savonije 1983, Joss, Rappaport, & Lewis 1987, and Rappaport et al. 1995). The value of the final core mass when the donor detaches from its critical Roche lobe is largely governed by the mass-transfer rate.

Eventually the donor loses so much mass that its total mass becomes comparable to the mass of the core itself. The remaining hydrogen-rich envelope contains so little mass that it is not sustainable (see Table 1 for values of m_{env}[4]). Since the largely adiabatic temperature gradient can no longer be supported, the envelope rapidly contracts towards a radiative equilibrium configuration. Mass transfer ceases and the donor subsequently consists largely of a helium core ($0.15 \lesssim (M_c/M_{\odot}) \lesssim 0.45$) on top of which resides an extremely thin hydrogen-rich envelope ($m_{env} \gtrsim 10^{-2} M_{\odot}$). The donor quickly moves to the left in the HR diagram at roughly constant luminosity. This important phase in the evolution which lasts from between $\sim 10^6$ to 10^8 years corresponds to the nearly horizontal parts of the tracks seen in Figures 1-6. The donors' radii can decrease by between one to two orders of magnitude. Hydrogen burning continues and the value of m_{env} can be substantially reduced (to evaluate this reduction compare the values of m_{env} in Tables 1 & 2). Since the core is always much more massive than the envelope, the core mass is almost constant during the horizontal phase and enforces a more or less constant rate of burning (i.e., a constant L_{nuc}) until the maximum value of T_e is attained. This value is largely governed by the core mass itself. Larger m_c's have higher luminosities and smaller (degenerate) radii and thus their values of $T_{e,max}$ are higher. The turnaround in T_e also leads to a precipitous decrease in the bolometric

[4] m_{env} is defined as the mass below the donor's surface above which the value of X is greater than zero.

luminosity and an abrupt increase in the ratio of L_g/L_{nuc} (the ratio increasing by more than a factor of 100). Further contraction of the envelope leads to (partial) adiabatic heating of the H-rich layer just above the H-depleted core. Depending on the core mass and metallicity, the H-burning shell can either: (i) undergo a mild thermal readjustment; or, (ii) undergo a H-shell flash (unstable CNO burning). If the hydrogen re-ignites, the donor sometimes expands so much that it fills its Roche lobe causing further mass transfer (in contrast to the present work, this possibility was not accounted for in the models of DSBH). Eventually the thermonuclear runaway is quenched and the donor's envelope collapses. It is possible for the donor to go through several cycles before nuclear burning is permanently extinguished (an extensive discussion of the details and a comparison with previously published results can be found in §3.2). After the final flash, the donor is destined to cool and approach its zero-temperature configuration.

Tracks corresponding to "intermediate mass" cores (see Figures 1-6) experience strong H-shell flashes. While the intermediate-mass cores do experience significant (multiple) thermal pulses, the low-mass cores are relatively unaffected. The reason that they do not experience runaways is probably due to the fact that their interiors tend to be colder and since pp burning is less sensitive to temperature, local nuclear energy generation cannot raise the temperature sufficiently quickly to induce a runaway. For the higher mass cores, the growth time of the burning instability and the thermal relaxation time of the envelope are comparable and thus unstable burning is quickly quenched.

After the "thermal pulse" phase is complete, the temperature in the envelope has risen sufficiently (especially for the low-mass cores) that the ratio of L_g/L_{nuc} has dropped below unity. Thus the cooling phase of HeDD's is different from that of CO DD's in that H-burning (via the pp-chain) can constitute an important fraction of the radiated energy for many billions of years. The inferred cooling times can be significantly different compared to models for which nuclear burning has been neglected (the importance of this phenomenon was first noted by DSBH). Even up to a Hubble time after the detachment of the donor from its Roche lobe, we find that the ratio of L_g/L_{nuc} remains below unity for many of our low core-mass cases (e.g., $m_c < 0.25 M_\odot$; Z = 0.02). For our highest core-mass cases, the ratio is < 1 for more than 1 Gyr. Consequently the low-mass DD's can have considerable thermal energy (i.e., finite entropy) even after a Hubble time (see also Figure 15). The retardation of cooling can have a significant effect on determining the ages of LMBP's (see §4).

3.1.1. Metallicity Dependence

The dependence of the evolution on the metallicity is illustrated in Figure 7. One set of curves (for each of the three metallicities) corresponds to donors whose masses are equal to $1M_{\odot}$ and whose values of $m_c = 0$ at the onset of mass transfer. The other set corresponds to the $m_c = 0.20M_{\odot}$ cases. Because the low-metallicity models tend to be hotter and smaller in radius, they evolve more quickly than their high-metallicity counterparts. Consequently the $Z = 0.0001$ case evolves sufficiently quickly (relative to the mass-transfer timescale) that it can create a core and ultimately evolves to become a HeDD. The $Z = 0.004$ donor starts to form a core (and temporarily attains higher T_e's) but ultimately loses too much mass and evolves to ever decreasing luminosities and temperatures. For the $Z = 0.02$ case, the mass transfer timescale is much shorter than the nuclear one and further growth of the core is stymied. The $m_c = 0.2M_{\odot}$ tracks lead to the formation of well-developed cores and ultimately HeDD's. The $Z = 0.0001$ track is initially hotter and more luminous than the higher metallicity ones. It experiences a vigorous shell flash while the $Z = 0.004$ model experiences a mild thermal pulse. A very mild thermal readjustment is also visible in the track of the $Z = 0.02$ model. Once the models descend the cooling branch for the final time, we see that the lowest metallicity models are also the smallest in radius. The same qualitative behavior is observed for the tracks of systems with initially higher-mass donors. The masses for which shell flashes can occur are also sensitive to the metallicity and this dependence will be addressed in §3.3.

3.1.2. Orbital Periods

Sample results of the evolution of P_{orb} with respect to the mass of the donor are shown in Figures 8 & 9. In Figure 8 all of the curves correspond to an initial donor mass of $1.5M_{\odot}$ with $Z = 0.02$ and various values of X_c and M_c. In Figure 9 all of the curves correspond to an initial donor mass of $1.5M_{\odot}$ with $Z = 0.0001$. There is a distinct bifurcation in the behavior of the orbital periods (this phenomenon has been investigated in great detail by PS, SEG, and PRP). Donors that ascend the RGB develop well-defined cores, become larger in radius and naturally evolve to higher periods. Donors for which mass loss is very rapid, evolve to smaller radii and P_{orb}'s. The orbital period reaches a minimum value as the donor evolves towards the degenerate branch (and their radii increase). We note that it is possible for the minimum period to be as short as 8 minutes (see PRP and NR) but the minimum value that we calculate based on our grid of initial conditions is ~ 20 minutes. Periods as short as these occur because the donors are very H-depleted and electron degenerate. As was observed in Figures 1 - 6, the same systems that evolve above the bifurcation limit are

the same ones for which we see the orbital periods increasing. As will be shown in §3.4, there is a strong correlation between the final orbital period ($P_{orb,f}$) and both the initial orbital period ($P_{orb,o}$) and m_f for donors that have well-developed cores. We also see that binaries that develop cores close to the classical helium-flash value (i.e., $\sim 0.46 M_\odot$) evolve to extremely long orbital periods in excess of 10^4 hours. It is also interesting to note that the initial range of P_{orb}'s for which the bifurcation occurs is moderately dependent on the metallicity. For example, taking $M_{2,o} = 1 M_\odot$, $M_1 = 1.4 M_\odot$, and $Z = 0.02$, we find that the bifurcation occurs between $13 \lesssim P_{orb,o} \lesssim 16$ hours and for $Z = 0.0001$ we find the range to be $8 \lesssim P_{orb,o} \lesssim 11$ hours.

Since the bifurcation limit is a very sensitive function of the assumed input physics it is not surprising that the assumption of fully conservative mass transfer (i.e., $\beta = 1$) leads to different limits. We analyzed the evolution of a large number of representative systems ($Z = 0.02, 0.0001$) assuming conservative mass transfer. The evolutionary tracks of the donors that evolve well above the bifurcation limit are qualitatively very similar to the corresponding cases calculated assuming completely non-conservative mass transfer. We see that in most instances the effect on P_{orb} and on the evolutionary properties of the donor is relatively small. For example, at a given mass, the orbital periods always agree to within $\sim 40\%$ (the maximum deviation occuring for the largest periods) and the final donor masses at the point of Roche-lobe detachment from the RGB vary by only a few percent. A typical case corresponding to $M_{2,o} = 1.0 M_\odot$, $m_{c,o} = 0.135 M_\odot$, and $Z = 0.02$ is shown in Figure 10. The evolutionary tracks of the donors in the HR diagram for these two extreme cases are offset during the donors' transition from the RGB (end of mass-loss) to the final cooling phase. It should also be noted that the physical properties (e.g., internal thermal profile) of donors undergoing conservative and non-conservative mass transfer are also very similar. Because of the sensitivity of the bifurcation limit to the physical inputs, we find that donors undergoing conservative mass transfer can be less evolved at the onset of mass loss and still produce HeDD's (e.g., $X_c = 0.05$ as opposed to $X_c = 0.0$ for $M_{2,o} = 1.5 M_\odot$ and $Z = 0.02$). The same trend holds true for the low-metallicity case ($Z = 0.0001$).

3.1.3. Interior Properties

For systems that evolve above the bifurcation limit, the values of the central temperature (T_c) and central pressure (P_c) rise monotonically while the donors are ascending the giant branch. Once mass transfer stops, the magnitude of P_c continues to increase gradually due to the contraction of the core and envelope, and the central temperature drops as the donor cools. One exception occurs when donors undergo shell flashes. For those cases, the

value of T_c can increase by a few percent but the effect is minimal. The temperatures inside the cores are not sufficiently high for neutrino fluxes to account for significant energy losses. Neutrino losses are completely unimportant except for high mass cores ($\gtrsim 0.4 M_\odot$). We also note that crystallization does not occur in the interiors of any of our models and is not likely to occur for any model that is allowed to cool for a Hubble time. This result is consistent with the analysis of the cooling of pure-helium ($Z = 0.003$) degenerate dwarfs by ND who found that these faster cooling models never crystallize within a Hubble time (see also HPa).

3.1.4. Mass-Transfer Rates

The mass loss rates from a representative set of donors ($M_1 = 1.4 M_\odot$) with a solar metallicity is shown in Figure 11. Note that if we assume that the accretor is a neutron star, some phases of the evolution (for certain initial conditions) lead to super-Eddington luminosities (corresponding to $\dot{m}$'s of $\gtrsim 2 \times 10^{-8} M_\odot$ yr^{-1}). A potentially important and observable feature of these evolutions results from the fact that the donors can become detached temporarily while evolving up the RGB (they correspond to the relatively pronounced dips seen in the curves). Whether or not this phenomenon occurs primarily depends on the evolutionary history of the envelope's convective zone; if a large hydrogen abundance gradient (or discontinuity) exists and if the H-burning shell passes through it, then the donor will contract on its Kelvin-Helmholtz timescale and mass transfer will cease temporarily. After the shell becomes equilibrated, the donor resumes its expansion causing mass transfer to recommence. This phenomenon occurs in models for which $0.05 \lesssim m_{c,o}/M_\odot \lesssim 0.25$ ($Z = 0.02$; see Figure 11), and we find that the range decreases with decreasing metallicity.

3.2. Hydrogen Shell Flashes and the Cooling of HeDD's

After the donor has evolved horizontally in the HR diagram and reaches its maximum value of T_e, it begins to descend the cooling branch (i.e., evolving towards lower luminosities and effective temperatures). However, as the envelope[5] continues to contract, the temperature at the base of the envelope (adjacent to the He-rich core) can rise due to partial adiabatic compression. If the density of the gas above this layer is sufficiently high that radiative transport cannot efficiently transport the heat outwards, a temperature inversion can occur. Given the extreme sensitivity of the CNO cycle to temperature and the inability

[5]We defined the mass of the envelope m_{env} to be the mass of those layers directly below the surface that contain a non-zero abundance of hydrogen.

of the outer layers to transport the heat sufficiently quickly, a thermal runaway can ensue. Typically shell flashes develop in a layer of H-rich gas that is only mildly electron degenerate ($\Psi \equiv \mu_{electron}/(kT) \approx 0$).

As has been shown by a number of authors (e.g., Kippenhahn & Weigert 1967, Webbink 1975, Iben and Tutukov 1986 [IT], DSBH, SEG, ASB, PRP) the envelope can, under certain conditions, be thermally unstable and one or more vigorous hydrogen shell flashes can occur. There is considerable disagreement however concerning the range of helium core masses for which shell flashes occur and the amount of hydrogen that resides in the envelope before and after the flashes. Many of these differences can be attributed to marked differences in the treatment of the physical processes within the donor star and the secular evolution of the binary itself). One of the first investigations of the evolution of He-rich dwarfs was carried out by Webbink (1975) who evolved extremely low-mass main-sequence stars (a few tenths of a solar mass) for many Hubble times until they turned off the RGB. He found that some of them experienced mild H-shell flashes. Alberts et al. (1996) investigated the properties of J1012+5307 by evolving low-mass HeDD's ($\sim 0.25 M_\odot$) and found that none of the models experienced shell flashes. The models of BA and HPa showed nuclear burning to be insignificant during the evolution of the remnant. This is probably due to the fact that the H-rich envelopes that they used were not evolved from the RGB, but instead specific values of m_{env} were adopted. HPa used the $\sim 0.3 M_\odot$ HeDD model of IT for which the envelope mass was $3 \times 10^{-4} M_\odot$. BA considered a wide range of possible masses such that $3 \times 10^{-4} \lesssim (m_{env}/M_\odot) \lesssim 1 \times 10^{-8}$. These envelope masses are very small compared to the ones calculated to using more recent self-consistent binary evolution models and this probably explains the discrepancy. DSBH were the first to point out the importance of nuclear burning in retarding the cooling of HeDD's but their method of calculating starting models was obtained by rapidly stripping mass from a star ascending the RGB. Since their calculations did not pertain to the evolution of a binary system, they did not allow for the possibility of mass-loss from the donor during H-shell flashes. Nonetheless, they concluded that shell flashes (for a solar metallicity) can occur for a HeDD mass range of $0.21 \lesssim M/M_\odot \lesssim 0.3$. The results of SEG were based on a self-consistent binary evolution calculation for low-mass HeDD's ($\leq 0.25 M_\odot$) and they showed that some models could overflow their Roche lobes during shell flashes and further determined the mass dependence for several metallicities ($0.003 \leq Z \leq 0.03$). For $Z = 0.02$ they found that the minimum mass of a HeDD that would undergo shell flashes was $0.192 M_\odot$. The occurrence of shell flashes causing mass transfer was also noted by PRP who evolved a grid of solar metallicity models under the assumption that $\beta = 0.5$. ASB recently revisited the issue of shell flashes and their effects on the cooling of solar metallicity dwarfs. They adopted the method of DSBH to obtain starting models (i.e., rapid mass loss from RGB stars). They showed that chemical diffusion can play

an important role in inducing shell flashes and they find that the mass range for which flashes occur is considerably wider than previously thought (i.e., $0.18 \lesssim m_f/M_\odot \lesssim 0.41$). This has the net effect of accelerating the cooling for models in this mass range. It should be noted, however, that diffusion is an extremely fragile process and that turbulence can mitigate its effects.

Our computations do not match any previously published results but share many of the distinct behaviors reported in those papers. For example, we find a finite range of remnant masses for which hydrogen shell flashes can occur and that this depends quite strongly on metallicity. In this regard our results are in reasonably good agreement with DSBH (for a solar metallicity we find that flashes occur for masses in the range of $0.21 \lesssim m_f/M_\odot \lesssim 0.28$). But we also examine how this range depends on the donor's metallicity. For extremely metal-poor donors ($Z = 0.0001$), we find that flashes occur in a substantially higher mass range of $0.30 \lesssim m_f/M_\odot \lesssim 0.36$. Similar to the findings of SEG and PRP, we find that multiple "cyclic" shell flashes are possible (also reported by DSBH, and ASB) and that in some cases, the HeDD overflows its Roche lobe causing mass accretion onto the compact companion.

One of the important distinguishing features between sets of models pertains to differences in envelope masses. The earlier models tended to have very small values of m_{env} while the ones calculated using binary models tended to have much larger values (at least at the point where the donor turned off from the RGB). For example, SEG typically found (initial) envelope masses of between $1 - 6 \times 10^{-2} M_\odot$ while DSBH found masses of between $\sim 2 - 50 \times 10^{-3} M_\odot$. Smaller values were calculated by ASB who chose for each case to tabulate their values at the maximum effective temperature; they found envelope masses of between $\sim 0.7 - 10 \times 10^{-3} M_\odot$. Our range of envelope masses places us between the higher-mass values of PS ($0.01 - 0.02 M_\odot$) and SEG, and the lower-mass ones of IT, BA, DSBH, and ASB. Our *final* values of m_{env} (determined at $\log(L/L_\odot) = -2$) can be accurately quantified using a power-law formula that is a function of the mass of the HeDD (m_f) and Z (see §3.3). For a solar metallicity, we find that the final values lie in the range of $0.0005 \lesssim m_{env}/M_\odot \lesssim 0.015$. The values are only weakly dependent on the initial masses of the donor ($M_{2,o}$) and the accretor ($M_{1,o}$).

The evolution of a donor whose initial properties at the onset of mass loss correspond to $M_{2,o} = 1.0 M_\odot$, $m_{c,o} = 0.15 M_\odot$, and $Z = 0.02$ is shown in the HR diagram (Figure 12). After the donor detaches from its Roche lobe (point 1), it evolves at almost constant luminosity until it reaches its maximum effective temperature (point 2). It then begins its descent down the cooling track but experiences a thermal instability corresponding to point 3 in the figure. The resulting thermal pulse causes the luminosity to increase and readjust. At point 4 in the figure, the donor is sufficiently large that it fills its Roche lobe thereby causing a brief episode

of mass transfer during which time its radius is almost constant (because $\Delta m/M_2 << 1$). This phase of mass transfer is denoted by the dotted line in Figure 12. At point 5, the donor detaches and begins a new phase of cooling. Along the way it suffers further thermal instabilities and at point 6 it descends the cooling track at approximately constant radius. During the mass loss phase, $\sim 0.00032 M_\odot$ is lost from the envelope. Although this is a small amount of mass, it is a non-negligible fraction of m_{env}. It is the mass and composition of the envelope that will ultimately govern the cooling evolution of the HeDD. Roche lobe overflow does not occur for the majority of the H-shell flashes that we computed, but it cannot be neglected.

It is interesting to note that if thermal instabilities do occur, they are initiated for very similar values of luminosity (assuming a fixed metallicity) and are only weakly dependent on the initial mass of the donor. This property can be seen in Figures 1-6, and is evident in Figures 13 and 14. In Figure 13 the luminosity is plotted against the elapsed time defined from the point where the initial detachment of the donor from its Roche lobe (near the RGB) occurs. For all curves, the initial mass of the donor was $M_{2,o} = 1 M_\odot$ and the metallicity was solar. The five curves correspond to $m_{c,o}$'s ranging from $0.05 M_\odot$ to $0.25 M_\odot$ in increments of $0.05 M_\odot$. The $0.05 M_\odot$ case is a good example of a multi-cyclic flash for which the donor experiences numerous thermal instabilities. These flashes persist for ~ 0.25 Gyr. We immediately see that these flashes can have a profound effect on the estimation of the ages of *young* pulsars based on the cooling times of the donors. The $m_{c,o} = 0.10 M_\odot$ case produced a HeDD with a higher mass ($0.231 M_\odot$ compared to $0.216 M_\odot$) and experienced two significant flashes at a much earlier age. The only other model that produced an unequivocal example of hydrogen shell flash corresponds to the $m_{c,o} = 0.15 M_\odot$ case. The higher (initial) cores mass cases ($m_{c,o} = 0.2 M_\odot$, $0.25 M_\odot$) experience mild thermal pulses but no unstable hydrogen burning. The corresponding evolution of the radius of $1 M_\odot$ donors ($Z = 0.02$) is presented in Figure 15. The radius of the donors experiencing shell flashes increases dramatically during the event(s), while weak thermal pulses result in small readjustments.

Figure 14 illustrates the evolution of the luminosity for solar metallicity models but for which the initial donor mass is $1.5 M_\odot$. The $m_{c,o} = 0.05 M_\odot$ case corresponding to a final HeDD mass of $0.209 M_\odot$ does experience a thermal pulse but avoids unstable burning. The next three values of core mass $m_{c,o} = 0.10, 0.15, 0.20 M_\odot$ do experience vigorous shell burning events. For each case, the events are initiated in the same range of luminosities as was seen for the $1 M_\odot$ donors. In fact, for all initial donor masses with solar metallicities we find that thermal instabilities are initiated for luminosities in the range $-0.6 \lesssim \log(L/L_\odot) \lesssim -0.2$.

In Figure 16 hydrogen shell flashes are compared for all three metallicities under the assumption that the initial donor mass was $1 M_\odot$ and that the initial core mass was $0.15 M_\odot$.

All three cases exhibit shell flashes with the metal poor donor undergoing flashes after approximately 1.5×10^7 yr. Although the masses of the HeDD's are not the same, the lower metallicity models evolve faster, in general, and thus experience shell flashes earlier and subsequently cool more quickly. The solar metallicity model undergoes a flash at a later time (6×10^7 yr) and cools more slowly. This figure also shows that the critical luminosities for which thermal instabilities occur is very metallicity dependent. Low metallicity models experience (the first) thermal pulses at much higher luminosities. We find that shell flashes for $Z = 0.02$ are initiated in the range of $-0.6 \lesssim L/L_\odot \lesssim -0.2$, and for $Z = 0.0001$ occurs for the range of $0.3 \lesssim L/L_\odot \lesssim 0.9$. Another difference that occurs for low-Z models is that some of the relatively low-luminosity H-shell flashes result from unstable pp burning (as opposed to CNO burning).

In Figure 17 we examine the cooling evolution of the donor as a function of its age from the time that it detaches from its Roche lobe (after evolving off of the RGB). For all curves, the initial mass of the solar metallicity donor at the onset of mass transfer is $1M_\odot$. The final masses of each of the HeDD's are labeled adjacent to the corresponding curve. The evolution is expressed in terms of the thermal bloating factor f where $f = R_2/R_o$. R_o is the radius of a zero-temperature star (Zapolsky & Salpeter 1969) composed purely of He and having the same mass as the donor. In the limit of an infinite cooling time, f will approach unity. As has been noted by many authors (e.g., IT and ND), He-rich dwarfs cool much more slowly then their CO counterparts. Figure 17 also reveals that higher-mass HeDD's cool faster than the low-mass ones. For example, after 5 Gyr, the $0.332M_\odot$ HeDD has contracted to within the $\sim 10\%$ of its zero-temperature radius while the $0.216M_\odot$ model is still bloated by $\sim 35\%$ (note that differences in the masses of the H-rich envelopes have not been taken into account but that this would not change the conclusions). As noted previously, low-mass HeDD's derive a substantial fraction of their luminosity from nuclear burning in their envelopes. This is clearly demonstrated in Figure 14 for the $0.209M_\odot$ HeDD track where we see that its luminosity is much larger than that for the other models when compared at specific (late) ages.

3.2.1. Shell Flash versus Thermal Pulse

Detailed analyses of the evolution of two different outcomes of a thermal instability (a vigorous hydrogen flash and a mild thermal pulse) are shown in Figures 18 and 19, respectively. In both figures panel a) shows the evolution of the HeDD in the HR diagram and panel b) depicts the temporal evolution of its temperature profile. As can be seen in Figure 18 a), the intermediate metallicity donor ($Z = 0.004$) with an initial mass of $1.5M_\odot$

and core mass of $0.10M_{\odot}$ experiences a shell flash but does not overflow its Roche lobe. Various critical junctures in the evolution are denoted by numbered dots in panel a). The elapsed time (and other properties) between each of these points is also listed in Table 3a. The evolution of the internal temperature of the donor for each of the corresponding points in panel a) is shown in Figure 18 b). The temperatures are plotted with respect to the stellar mass fraction $\log(1 - M_r/M)$ where M_r is the mass residing inside of a shell radius r. At point 1, corresponding to a value of $\log T_c = 7.63$, T_e has reached its maximum value. The interior is reasonably isothermal up to a mass fraction of $\sim 99\%$. As the donor cools, the outer layers cool quickly (compare points 1, 2 and 3) while the interior remains at more or less constant temperature (the elapsed time between points 1 and 3 is much shorter than the cooling timescale of the interior). However at point 3, the temperature near the base of the envelope reaches a minimum value and (partial) adiabatic heating occurs. Between points 3 and 4 the luminosity of the donor increases and so does the temperature near the base of its envelope. A very clear temperature inversion takes place and is accelerated by the energy generation produced by pp-burning. At point 5 the inversion is extremely pronounced and the maximum temperature in the shell is nearly 4×10^7K. At this point CNO burning completely dominates energy production and leads to a very significant further increase in the temperature of the shell ($\sim 5 \times 10^7$K). We also start to see the effects of this temperature inversion since heat is flowing both towards the interior and towards the surface. The increase in nuclear burning leads to a very substantial increase in the surface luminosity (more than two orders of magnitude). The onset of CNO burning creates such a large flux of energy flowing outwards that the layers immediately above the burning shell are unstable against convection and a convective front moves out towards the surface. This causes hydrogen rich material to be mixed into the burning zone. After a further thermal readjustment (recession of the convective zone), T_e decreases and the envelope expands until the HeDD reaches its maximum radius (point 7). Burning at the base of the envelope is still vigorous and the amount of available fuel decreases. Heat continues to flow inwards and even at point 8 we see a very significant increase in the temperature in the outer 2% of the mass of the He-rich core. It is also interesting to note that just before the donor reaches point 8, it experiences two more thermal pulses. The HeDD then begins another descent down the cooling branch which is interrupted by a further weak thermal pulse (point 9). After the formation (and recession) of a small convective zone near the base of the envelope (point10), the HeDD continuously cools and becomes increasingly electron degenerate.

Figure 19 depicts the evolution of a $1.5M_{\odot}$ donor with $Z = 0.004$ and an initial core mass of $m_{c,o} = 0.25M_{\odot}$ (see Table 3b for the corresponding numerical data). This model experiences a mild thermal instability but not a hydrogen shell flash. At point 1 the donor evolves horizontally in the HR diagram and we see a very steep temperature gradient in the

outer 1% of its mass. The interior is approximately isothermal and significantly electron degenerate. As the donor evolves we see that the temperature in the outer layers drops and the temperature gradient is less steep. This latter result can be explained by the fact that energy transport in the outer layers is being dominated by radiation. This trend continues and at point 5 we start to see a significant drop in the temperature in the outer 10% of the mass of the HeDD. Between points 7 and 8 sufficient time has elapsed for the value of T_c to drop by $\sim 20\%$. However, due to continued collapse of the envelope, the outer 0.3% of the donor undergoes a slight thermal readjustment (but it does not lead to a temperature inversion since the temperatures are too low to ignite significant nuclear burning). At point 10 the donor is descending the cooling branch and the value of $\log L/L_\odot$ has decreased to ~ -1.7. Whether or not a donor will experience a shell flash depends sensitively on its thermal (and nuclear) history and on assumptions pertaining to the input physics. We're presently investigating these issues (e.g., diffusion) in much more detail.

3.3. Envelope Masses

As mentioned in §3.1, the mass of the envelope (defined to be equal to the mass of those layers above the He-rich core containing any non-zero amount of H) continues to decrease due to nuclear burning after the donor detaches from its Roche lobe. By comparing the values of m_{env} in Tables 1 & 2 it is clear that the mass of the envelope can decrease substantially. The actual decrease can depend sensitively on whether or not a flash occurs and whether there is subsequent loss of envelope mass because of Roche lobe overflow.

The mass and composition of the envelopes play a paramount role in dictating the cooling timescales of HeDD's; this in turn affects our estimation of the ages of pulsars in LMBP's. This approach of inferring pulsar ages constitutes a very important and completely independent method when compared to the method used to derive their characteristic ages based on the measured spin-down derivatives (see §4 for a discussion). Our evolutionary calculations show that there is a reasonably well-defined dependence of m_{env} (determined at $\log(L/L_\odot) = -2$) on the metallicity and the mass of the remnant itself. We also find that the envelope mass is only weakly dependent on the initial donor mass. These claims are validated by Figure 20. The figure shows the dependence of m_{env} on the mass of the HeDD for the three adopted values of the metallicity. The symbols correspond to different initial donor masses (1.0, 1.5, and 2.0 $M_\odot$). For a fixed value of Z, the results show that m_{env} is negatively correlated with the mass of the remnant (a result noted by DSBH).

Based on these results we were able to obtain an extremely reliable fit for the mass of

the envelope:

$$m_{env} \;=\; 3.0 \times 10^{-5}\; Z^{-0.21}\; \left(\frac{m_f}{M_\odot}\right)^{-2.8} \quad M_\odot \tag{5}$$

with a coefficient of determination of $R^2 = 0.96$. We caution that the fit given by Equation (5) should not be extrapolated to values of m_f lower than the bifurcation limits for each respective metallicity[6]. Our computation of m_{env} yields values (for $Z = 0.02$) that fit in middle of the range reported (or adopted) in other papers. The reasons for the discrepancies arising in the different values of m_{env} can be traced to the sensitivity of the values on the input physics (e.g., nuclear cross-sections, screening factors, etc.), the method of solution (e.g., choice of the fitting point between the interior and the envelope), and assumptions concerning the prior evolution of the binary. The effects of shell flashes on reducing m_{env} more than that expected from the formula can be seen in Figure 20. Note that for $Z = 0.02$ we can see the effect very clearly for masses in the range of ~ 0.21 to $0.28 M_\odot$.

Finally we plan to examine the dependence of m_{env} and the cooling times on factors such as the treatment of convection, diffusion, and investigate other modes of angular momentum dissipation. We have investigated the effects of adopting the assumption of fully conservative mass transfer and we conclude that Equation (5) still yields a very good fit to the models. Obviously the same starting conditions can sometimes lead to very different evolutionary behaviors. For example, the $M_{2,o} = 1.5 M_\odot$, $X_{c,o} = 0.0$, $Z = 0.02$ case leads to three flash cycles for conservative transfer whereas completely non-conservative mass transfer does not produce a HeDD that undergoes thermonuclear runaways.

One of the key factors in determining envelope masses and post-RGB evolutionary behavior is the mass of the HeDD at the turn-off from the RGB. This mass is determined largely by the value of $M_{2,o}$, the degree of evolution of the donor at the onset of mass transfer, and the mode of angular momentum dissipation. One other factor that affects the evolution is stellar winds. Unfortunately the uncertainties in the mass-loss rate due to winds is substantial and depends on the exact phase of evolution (Willson 2002). To investigate a reasonable range of possible wind losses, we used a parameterized version of Reimers' formula (1975) for which

$$\dot{m}_{wind} \;=\; 4.0 \times 10^{-13}\; \eta\; \left(\frac{L_2}{L_\odot}\right)\; \left(\frac{R_2}{R_\odot}\right)\; \left(\frac{M_2}{M_\odot}\right)^{-1} \quad M_\odot \text{ yr}^{-1} \quad , \tag{6}$$

where η is parameter that was adjusted to have values between zero (no wind) and 10. We find that winds seem to have very little effect on the value of the envelope masses (as given

[6]We have calculated additional models near the bifurcation limit and found that the limit is $\lesssim 0.15 M_\odot$ for $Z = 0.02$ and $\lesssim 0.21 M_\odot$ for $Z = 0.0001$.

by Equation (5)) but do reduce the value of the final mass of the HeDD (i.e., m_f) for a given set of initial conditions at the onset of mass transfer. For example, the case for which $M_{2,o} = 1.0 M_\odot$, $X_{c,o} = 0.20$, and $Z = 0.02$, we find that $\eta = 1$ yields a $0.30 M_\odot$ HeDD (that does not flash) while $\eta = 10$ yields a $0.26 M_\odot$ HeDD (that does flash). Although this difference in behaviors does effect the value of m_{env}, we have seen that the effect is not substantial. We find that winds do on average reduce envelope masses but typically only by $\lesssim 15\%$ for $\eta = 10$. This is largely due to the fact that wind losses are small during the contraction phase. The time that the HeDD spends as a relatively high luminosity (and large radius) object is very short (see Figures 1 - 6) and thus, although $\dot{m}_{wind}$ is relatively high during this phase, the integrated mass loss is still small. The detailed results of this study will be reported elsewhere (Nelson & Dubeau 2004b).

3.4. $P_{orb,f} - m_f$ Dependence

The most striking feature of the evolution of our grid of systems is the bifurcation between evolutionary sequences. The bifurcation limit is very sensitive to the input physics, especially the mode of angular momentum dissipation that the binary experiences (see Ergma et al. 1998). As long as donors have a chance to form well-developed cores (i.e., they are well above the bifurcation limit), then there is a good correlation between P_{orb} and the value of m_f of the HeDD (see Rappaport et al. 1995, and references therein; ST). This correlation is primarily due to the fact that the radius of the donor as it leaves the RGB (and mass transfer ceases) is largely dictated by the value of m_c. Thus the Roche lobe radius (and hence the orbital period) at turnoff is largely dependent on m_c.

The derivation can be described as follows: Since $M_2 << M_{tot}$ for giant donors that are just about to collapse as they turn off the RGB, we can approximate their (volume-averaged) Roche lobe radius by the following formula (Paczyński 1971):

$$R_L = \frac{2}{3^{4/3}} \left(\frac{M_2}{M_2 + M_1} \right)^{1/3} A \; . \tag{7}$$

If we combine this equation for the Roche lobe, which we take to equal the radius of the giant donor, R_2, with the expression for Kepler's Third Law, we find the following well-known relation between the orbital period, P_{orb}, the donor mass, and the Roche-lobe radius:

$$P_{\rm orb} = \frac{9\pi}{\sqrt{2G}} \; R_L^{3/2} M_2^{-1/2} \; . \tag{8}$$

Because the envelope mass is much smaller than m_c and because the decrease in m_{env} as the remnant cools (and possibly experiences shell flashes) will not change m_c substantially, we

can set $M_2 \simeq m_c \simeq m_f$. Furthermore, $R_{L,f} \simeq R_{2,f}(m_c)$ and thus we can see from Equation (8) that P_{orb} can be expressed largely in terms of m_c (or equivalently m_f).

The relationship between $P_{orb,f}$ and m_f is shown in Figure 21 for all three metallicities. As is evident from the figure, there is a strong correlation between $P_{orb,f}$ and m_f for each of the metallicities. This relationship has been extensively analyzed by Rappaport et al. (1995); they chose to take an average over all metallicities (and mixing-length ratios) to obtain their final $P_{orb} - m_f$ relation. However, as noted by Ergma et al. (1998), donors that do not have well-developed cores at the onset of mass transfer will not obey a (universal) $P_{orb} - m_f$ relationship. We see this effect in our results (for the lowest values of m_c) for systems that are near the bifurcation limit. For donors that do develop substantial cores ($\gtrsim 0.25 M_\odot$) there is a strong correlation between $P_{orb,f}$ and m_f (see also TS who investigated two metallicities). Our results explicitly allow us to include the effects of metallicity in the $P_{orb,f}(m_f)$ relationship. We find that a good fit is obtained for

$$P_{orb,f} \;=\; 2.5\; Z^{0.3}\; 10^{10.7(m_f/M_\odot)}\;\; \mathrm{hr}\;, \tag{9}$$

with a coefficient of determination of $R^2 = 0.94$. This formula compares favorably with the results obtained by Rappaport et al. (1995). Using their best fit to the theoretical results, we find almost perfect agreement at the high-mass end ($\sim 0.45 M_\odot$) but we find that our P_{orb}'s are almost one-third lower for masses of $\simeq 0.25 M_\odot$. At even lower masses (i.e., those below which Equation [7] *cannot* be used), the discrepancy can exceed a factor of two. However, because of the very strong dependence of P_{orb} on m_c, this is equivalent to stating that their inferred values of m_f are only about 15% lower for values of $P_{orb} \simeq 2$ days (i.e., $\sim 0.03 M_\odot$ lower). Our results agree much more closely with those found by TS (they allowed for partial mass accretion by the NS and considered tidal coupling). According to Equation (9), the metallicity dependence can lead to deviations in the inference of the P_{orb}'s by as much as a factor of 5 (for extreme population differences). Since it is difficult to accurately evaluate the metallicity of any donor, this equation underscores the fact that inferences of m_f based on the measured P_{orb}'s must be treated with caution. We also find a reasonably good correlation between $P_{orb,f}$ and $P_{orb,o}$ for donors that have well-developed cores (i.e., well above the bifurcation limit). These results are shown in Figure 22. We see that for systems evolving near the bifurcation limit (i.e., small values of m_c), the final values of P_{orb} can be *much smaller* than would be expected from a simple extrapolation of the $P_{orb,f}(m_f)$ relationship. Finally we note that this formula is only applicable to fully non-conservative mass transfer and should be used for masses in the range of $\sim 0.25 - 0.4 M_\odot$ (i.e., $10 \lesssim P_{orb,f}(\mathrm{days}) \lesssim 500$ for solar metallicities, and $4 \lesssim P_{orb,f}(\mathrm{days}) \lesssim 100$ for extremely metal-poor donors).

4. Application to Selected Observations

Binary millisecond pulsars provide us with some of the best observational data with which we can test the theoretical predictions of the properties of HeDD's. Many HeDD's (and HeCO DD's) have been discovered in the past decade and several are found in these "recycled" pulsar systems. The original magnetic field of the neutron stars has decayed to $\lesssim 10^9$ G but the accretion of $\gtrsim 0.01 M_\odot$ of matter has spun them up to millisecond rotational periods (see Bhattacharya & van den Heuvel [1991] for a review). An estimation of the age of a pulsar can be obtained from the equation

$$t \;=\; \frac{P}{(n-1)\dot{P}}\left[1-\left(\frac{P_0}{P}\right)^{n-1}\right] \quad , \tag{10}$$

where P is the measured spin period, P_0 is the initial period, and $\dot{P}$ is the spin time derivative. The braking index is specified by n ($n = 3$ for dipolar radiation). If $P_0 \ll P$, then the characteristic age can be approximated by $\tau_{ch} = P/(2\dot{P})$. The cooling times of HeDD's provide us with a completely independent approach to inferring the ages of millisecond pulsars and can be used in conjunction with the pulsar's measured period and spin-down rate to constrain important properties such as P_0 (see HPb for a complete discussion of these issues).

Almost 100 recycled pulsars have been discovered to date (see, e.g., Camilo et al. 2000) and a large fraction of these are found in globular clusters. Galactic LMBP's have P_{orb}'s of between ~ 0.25 days to more than 1000 days (a period gap seems to exist between ~ 23 and 56 days). A much shorter-period class of BMSP's also exists for which $P_{orb} \lesssim 10$ hours and for which the donors are likely to have an extremely low mass of $\lesssim 0.03 M_\odot$ (see, e.g., Rasio et al. 2000 for a discussion). Perhaps some of these companions have undergone a period of ablation due to exposure to the electromagnetic radiation/relativistic winds emanating from the newly-born pulsars (Fruchter et al. 1988). Understanding the evolution of BMSP's located in globular clusters is complicated by the relatively high probability of dynamical encounters, in particular exchange interactions, that are likely to occur in the cluster cores. In what follows, we briefly analyze the theoretical predictions pertaining to several representative LMBP's. The evolution of GK Per will also be discussed since it may be a CV system that is evolving just above the bifurcation limit and may ultimately become a double-degenerate binary system[7].

[7]To date more than ten double-degenerate binaries consisting of at least one low-mass DD component ($\lesssim 0.45 M_\odot$) have been detected (Maxted et al. 2002). Unfortunately the masses of the components are not precisely known and many of these systems may have been formed via a completely different evolutionary channel.

4.1. PSR J1012+5307

The BMSP J1012+5307 ($P_{orb} \simeq 14.5$ hr) has been well studied (Lorimer et al. 1995) and its companion has been observed photometrically. van Kerkwijk et al. (1996) determine the effective temperature of the dwarf to be $T_e = 8550 \pm 25$K with an inferred $\log g = 6.75 \pm 0.07$. A later study by Callanan et al. (1998) allows for a much wider range of values ($T_e = 8670 \pm 300$K and $\log g = 6.31 \pm 0.2$). These observations provide us with a unique opportunity to confront spin-down theory with the observations (see, e.g., HPb for a discussion). Lorimer et al. (1995) used the spin-period derivative to estimate the pulsar's age (and hence the age of the companion) to be ~ 7 Gyr. HPb, using the envelope masses from IT, estimate the mass of the HeDD to be between $0.13 - 0.21 M_\odot$ and its age to be < 0.6 Gyr. They did not find nuclear burning in the envelope to be important and thus their estimated cooling age is relatively short. DSBH and SEG showed that the effects of nuclear burning on the inferred cooling ages of low-mass HeDD's (in particular) could be substantial. It was also noted by Ergma & Sarna (1996) that systems near the bifurcation limit that necessarily produce very low-mass HeDD's ($\lesssim 0.2 M_\odot$) would not have formed from donors that had well-developed cores and thus the use of a $P_{orb} - m_f$ relationship (such as the one derived in §3.4) would not be appropriate. The grid presented in this paper is too sparsely populated to infer the cooling age of J1012+5307, so we calculated additional tracks. Interpolating these results (and assuming a solar metallicity and that $T_e \simeq 8600$K) we conclude that the best fit for the companion corresponds to $\log L/L_\odot = -2.1 \pm 0.2$, $m_f = 0.17 - 0.18 M_\odot$, $t = 8 - 9$ Gyr, and $\log g = 6.5 \pm 0.1$. Our models reasonably fit the results derived by van Kerkwijk et al. (1996) but the ones derived by Callanan et al. (1998) are less constraining. The cooling age for this donor (which does not undergo a flash and thus does not overflow its Roche lobe) is in good agreement with the spin-down time inferred from the pulsar measurements. The importance of nuclear burning in these low-mass donors is clearly demonstrated and is the primary reason for the discrepancy between our results and those of HPb. Finally we note that if there were no H-rich envelope, the models of Nelson and Davis (2000) would imply that for $m_f = 0.18 M_\odot$, the cooling age would be much shorter (~ 0.5 Gyr).

4.2. PSR B1855+09

This system is composed of a 5.4 ms radio pulsar and a low-mass companion (inferred from the measured mass function) in a 295-hour circular orbit (Segelstein et al. 1986). This BMSP is rather unique in that the mass of the companion has been measured quite precisely using the Shapiro delay of the pulsar signal (Kaspi et al. 1994). The mass is found to be $\sim 0.258 \pm 0.02 M_\odot$ and the characteristic age of the pulsar is thought to be ~ 5 Gyr. The

companion has been detected and its effective temperature is inferred to be 4800 ± 800K (see van Kerkwijk et al. [2000], and references therein). This system is very important as an observational test of our understanding of the formation and evolution of HeDD's. The most stringent test concerns the relation between P_{orb} and m_f. In essence it allows us to test the accuracy of our computed relationship between the radius of the (RG) donor and its core mass at the point of detachment (assuming that the effects of shell flashes are properly evaluated). Based on our models and using the observed value of P_{orb}, we find that $m_f \simeq 0.25 M_\odot$ for a solar metallicity. If we reduce the metallicity slightly ($Z = 0.015$), we can obtain almost perfect agreement with the best estimate of m_f. The second test concerns the cooling time of the donor in comparison with the pulsar's characteristic age. Given the relatively thick envelopes expected for this mass and the importance of nuclear burning, most recent models imply a cooling time of $\gtrsim 10$ Gyr. While this is not in unreasonable agreement with the characteristic age, it does seem to imply that the envelope is too thick. The recent work of ASB who employed diffusion seems to resolve this issue. They conclude that the HeDD can cool to the observed within 4 Gyr. We did not evolve our models to such low temperatures, but an extrapolation reveals a cooling time of $\gtrsim 10$ Gyr. If the H-rich envelope were removed, the models of Nelson and Davis (2000) would imply that the cooling age could be much shorter (~ 3 Gyr). If we adopted an extremely low metallicity, it might also be possible to obtain a cooling time of 5 Gyr.

4.3. PSR J0437-4715

Another extremely important system is the LMBP J0437-4715 which has a nearly circular orbit and a $P_{orb} = 137.8$ hr (Johnston et al. 1993). It is also the closest LMBP at a distance of about 140 pc. Like PSR 1855+09, the Shapiro delay was used to determine both the mass of the HeDD ($0.236 \pm 0.017 M_\odot$) and of the pulsar ($1.58 \pm 0.18 M_\odot$; van Straten et al. [2001]). They also infer an inclination angle of $i = 42.75°$ which is consistent with the upper limit of 43° found by Sandhu et al. (1997). Based on our computations and assuming a solar metallicity, an extremely good fit to the observations can be obtained for $M_2 \simeq 0.23 \pm 0.01 M_\odot$. The characteristic age of the pulsar based on a precise measurement of the spin-period derivative yields an age of ~ 4.9 Gyr. Assuming an age of 5 Gyr, our cooling curves imply that $T_e \approx 8500$K and $\log L/L_\odot \approx -2.5$. However, based on the observations of Bell et al. (1995) it appears that the effective temperature is only ~ 4000K. The models of ASB (solar metallicity) seem to reconcile the spin-down time with the cooling time.

4.4. Ultracompact Systems

There are a number of LMXB's and recently discovered accreting millisecond (binary) pulsars that have ultrashort orbital periods ($\lesssim$ 60 minutes). The former group includes: 4U 1915-05 (50.0 min), 4U 1626-67 (41.4 min), 1850-0846 (20.5 min), and 4U 1820-30 (11.4 min); and the latter group consists of XTE J0929-314 (43.6 min), XTE J1751-305 (42.4 min), and XTE J1807-294 ($\lesssim$ 40 min). There are also several ultracompact CV's including V485 Cen (59.0 min), GP Com (46.5 min), CP Eri (28.7 min), V803 Cen (26.9 min), HP Lib (18.6 min), CR Boo (24.5 min), AM CVn (17.1 min), and ES Cet (10.3 min) (see, e.g., PRP and references therein). There are number of evolutionary pathways that could lead to the formation of these ultrashort-period systems, but it is clear that the donors must be moderately to severely hydrogen depleted (see, e.g., NRJ). As shown by a number of authors, including Tutukov et al. (1985), Pylyser & Savonije (1988, 1989), and NR, these systems can be formed by systems wherein the donor is close to TAMS at the onset of mass transfer (i.e., above the bifurcation limit). PRP and NR showed that LMXB's with periods as short as $\sim$ 8 minutes could be produced. Our smallest values of P_{orb} (corresponding to systems just below the bifurcation limit) can be a short as $\sim$ 20 minutes ($M_2 \sim 0.1 M_\odot$). We caution however that pressure ionization and Coulombic coupling can be very important in these low-mass models and for that reason we halted our evolutionary sequences when $M_2 \lesssim 0.1 M_\odot$. There is a strong correlation between the metallicity and the minimum value of P_{orb}. Metal-poor donors are considerably smaller than their solar metallicity counterparts and thus their P_{orb}'s are smaller (see Equation [8]).

4.5. GK Per

GK Per is a CV with a P_{orb} of 47.9 hr (Crampton et al. 1983). The optical companion is classified as a spectral type K2 IV (Warner 1976) and the compact accretor is a white dwarf. Based on the analysis of the X-ray pulse period and on evolutionary calculations of subgiants, Watson et al. (1985) estimated $M_1 \geq 0.72 M_\odot$ and that $M_2 \approx 0.25 M_\odot$. Using this as a starting point (and taking $Z = 0.02$), we find that only sequences (for $M_1 = 0.7 M_\odot$) that evolve just above the bifurcation limit can reproduce the observations. The 'best fit' is obtained for a $1 M_\odot$ donor whose initial core mass is $\sim 0.1 M_\odot$. By the time that M_2 is reduced to $0.245 M_\odot$, $\log L_2/L_\odot \approx -0.1$ and $T_e \approx 4600$K. These results are in good agreement with the luminosity class assignment and spectral type. We also find that the donor is likely to have a hydrogen surface abundance of $X_s \sim 0.6$ and that its He-core mass is $\sim 0.13 M_\odot$. Unfortunately, the value of the surface abundance of hydrogen is not sufficiently different from the primordial abundance that it could be used to test the theoretical predictions.

5. Summary

We have systematically analyzed the evolution of a grid of interacting binary systems that ultimately lead to the formation of He-rich DD's in either a detached or semi-detached state. Although parameter space is five dimensional ($M_{2,o}$, $m_{1,o}$, Z, $X_{c,o}/m_{c,o}$, $\dot{J}$), we have explored an important slice of it. The initial conditions were chosen so as to cover a wide range of realistic physical parameters and special attention was paid to maximizing the computational accuracy. Unlike previous investigations, we analyze the formation and properties of isolated (detached) HeDD's for masses up to the helium flash ($\sim 0.46 M_{\odot}$) and for all realistic metallicities ($0.0001 \leq Z \leq 0.02$).

As noted in several previous papers, there is a an extremely sharp bifurcation between donors that evolve to become giants whose cores subsequently cool as HeDD's, and those that continue to lose mass until they are reduced to planetary-mass sized objects. This bifurcation is very dependent on the assumed initial conditions and the input physics. We are currently investigating other portions of parameter space and also calculating a finer grid of models. All this is part of the MULTIGRID project (Nelson & Dubeau 2004a). The models calculated for this paper constitute part of an archive that is available for retrieval; a Web-server is also available so that specific tracks can be calculated on demand.

Several very interesting results have come out of this study (some of which confirm published claims and others which are complementary to previous work). The main findings can be summarized as follows:

1) The determination of the cooling times of HeDD's gives us a completely independent method of determining the ages of millisecond pulsars in LMBP's. As shown by HPb, the cooling age can in principle be used in conjunction with the measured pulsar spin-down times to constrain the initial spin periods of individual pulsars and possibly be used to comment on their magnetic-field decay times. This can only be accomplished if accurate inferences can be made as to the age of the HeDD companion based on its cooling evolution. Unfortunately this latter determination is problematic due to a number of uncertainties: (i) there is no precise consensus as to the envelope mass and composition of HeDD's; (ii) the importance of ablative or other phenomena that leads to a reduction in the envelope mass has not been rigorously investigated; and, (iii) the metallicity of the primordial binary needs to be well established. If the donor loses a significant fraction of its envelope (e.g., $\gtrsim 50\%$) during the contraction/cooling phase, this loss can greatly affect the predicted cooling times.

2) We find that nuclear burning is important in retarding the cooling process, especially for low-mass HeDD's (as noted by DSBH and SEG). Accounting for this burning corrects the discrepancy between the spin-down time and the cooling time of LMBP's such as PSR

J1012+53. However, there are other systems (e.g. PSR 1855) and some double (helium) degenerates (Yungelson et al. 2002) for which the cooling needs to occur on a shorter timescale in order to explain the observations. This can be accomplished if m_{env} is smaller than the values quoted in this paper, but is possible that the value of m_{env} decreases due to effects other than nuclear burning after the donor has detached from its Roche lobe. We are currently examining the effects of ablation on the envelope structure and cooling times. We know, for instance, that if the envelope is completely removed (yielding pure helium HeDD's) then the cooling times would be much shorter (see, e.g., Nelson and Davis 2000). Alternatively, ASB have shown that the diffusion of hydrogen is a very good candidate to reconcile pulsar spin-down times and the inferred cooling ages.

3) If the cores are well-developed ($m_c \gtrsim 0.10 M_{\odot}$) at the onset of mass transfer, then the value of the final orbital period of a BMSP can be reasonably accurately predicted based on the final mass of the HeDD and its metallicity. Since $P_{orb,f} \propto Z^{0.3}$, this implies that for a given HeDD mass, the value of P_{orb} for systems in globular clusters should be a factor of 2-5 times smaller than for systems in the galactic plane (assuming that the systems form and evolve in a similar manner). This is a very significant difference but it is difficult to verify because: (i) the mass of the HeDD needs to be determined very precisely due to the very strong dependence of $P_{orb,f}$ on m_f; and, (ii) the relatively high probability of exchange interactions/captures for those metal-poor systems residing in the cores of globular clusters. Based on the available observational data, we can only conclude that there is no statistical inconsistency.

4) We confirm that all HeDD's experience some form of thermal pulse and that vigorous shell flashes only occur for a finite range of masses (e.g., similar to the results found by DSBH for solar metallicities), and we show that this range is strongly correlated with the metallicity of the donor. Furthermore shell flashes can alter cooling times on both the short- and long-terms (and also lead to renewed episodes of mass accretion by the NS). On the short term they can delay cooling (we assume that the "zero-point" in age is taken to be the point where the donor turns off the RGB and mass-loss ceases), and in the long term the reduction of the envelope's H-rich mass can lead to increased cooling. The first effect could potentially be quite important when trying reconcile the characteristic (spin-down) ages of very young pulsars.

5) We find that for certain ranges of initial conditions (see, e.g., Figure 11) that mass transfer can temporarily cease if there is a substantial gradient (or discontinuity) in the hydrogen abundance profile in the envelope of the donor as it ascends the RGB. This is true for all metallicities but occurs for a wider range of initial conditions in higher metallicity systems. The donor initially shrinks within its critical Roche lobe and then expands until RLOF

resumes. At the point where mass transfer just stops, the neutron star would have already accreted sufficient matter and would 'turn on' as a recycled pulsar. The pulsar could then be detected at radio wavelengths and we predict that the measured mass function would likely be relatively large compared to what would be expected for LMBP's that are old and thus in the cooling phase. Adopting $Z = 0.02$, we find that the mass of the donor during this phase could be in the range of $0.2 \lesssim (M_2/M_\odot) \lesssim 0.8$. The interesting question is whether the pulsar would have any effect (e.g., ablation) on the evolution of the donor and thus on the binary system itself. If ablation or the radio ejection of matter (see Burderi, D'Antona & Burgay 2002) were important and prevented the donor from re-filling its Roche lobe or caused a significant amount of mass loss from the donor, then the formation of BMSP's containing intermediate-mass HeDD's ($0.25 \lesssim m_f/M_\odot \lesssim 0.3$) would be inhibited. If this scenario is correct, then 'gap' in the distribution of P_{orb}'s coincident with the observed gap of between ~ 20 to 60 days can be reproduced (Nelson 2004a). Moreover, if the pulsar can effectively stymie further mass accretion by ejecting mass from the binary system, then we would expect these systems to be reasonably long-lived BMSP's for which the donor fills a large fraction of its Roche lobe. This may lead to eclipsing phenomena such as that observed in J1740-5340 (D'Amico et al. 2001) [it should be noted that this pulsar is located in NGC6397 which is an extremely metal-poor globular cluster and the binary system has probably undergone an exchange interaction/tidal capture given its distance from the cluster's core (see Nelson 2004b for a discussion of this effect on the evolution of J1740-5340)]. Such systems would have a reasonably high probability of detection and confirmation of their existence would be enormously beneficial to our theoretical understanding of the evolution of interacting binaries containing pulsars.

Developing a self-consistent picture that explains the relative numbers of LMXB's and LMBP's and their orbital period distribution is absolutely essential if we are to understand the formation and evolution of low-mass, interacting binaries containing compact objects. We plan to use our computed results (with finer resolution for systems near the bifurcation limit) to carry out binary population syntheses (BPS's) to better understand issues such as the apparent gap in the orbital period distribution of BMSP's. Another important issue that will be addressed by a BPS study concerns the relatively large number of BMSP's whose donors apparently had initial properties placing them close to the bifurcation limit. If the explanation is that the progenitor binaries were formed with initial conditions close to this limit (after the formation of the neutron star), then we would expect an equivalently large number of systems just below the limit (i.e., the ones that can evolve to ultrashort periods because their donors are helium rich). This may account for the ultracompact accreting millisecond pulsars that have been recently discovered. Our preliminary analysis suggests that these two types of systems are closely related to each other.

This research was supported in part by an operating grant from the Natural Sciences and Engineering Research Council (NSERC) of Canada. L.A.N. would like to acknowledge the Canada Research Chairs program and K.M. and E.D. would like to thank NSERC for the USRA awards that they received. We are grateful to Jonathan Benjamin and Kevin Thibault for their technical assistance, and to S. Rappaport, Ph. Podsiadlowski, and M. van Kerkwijk for numerous discussions. Finally we are greatly indebted to the referee for extensive suggestions that led to significant improvements in this paper.

Note Added in Manuscript: In a much earlier version of this paper (2001) we had not fully taken into account the effects of superadiabaticity in the outer layers of the interior (i.e., just below the fitting mass that delineates the interior from the envelope). Although this problem did not affect our low-luminosity donors, it had a noticeable effect on the evolution of higher core-mass cases. We recalculated the grid thereby addressing this issue completely.

REFERENCES

Alberts, F., Savonije, G.J., & van den Heuvel, E.P.J. 1996, Nature 380, 676.

Alexander, D.R., & Ferguson, J.W. 1994, ApJ, 437, 879.

Althaus, L.G., & Benvenuto, O. G. 1997, ApJ, 477, 313.

Althaus, L.G., Serenelli, A.M., & Benvenuto, O.G. 2001, MNRAS, 324, 617 [ASB].

Bell, J.F., Bailes, M. & Bessell, M.S. 1995, Nature, 364, 603.

Benvenuto, O.G., & Althaus, L.G. 1998, MNRAS, 293, 177 [BA].

Bhattacharya, D., & van den Heuvel, E.P.J. 1991, Phys. Rep., 203, 1.

Burderi, L., D'Antona, F., & Burgay, M. 2002, ApJ, 574, 325.

Callanan, P.J., Garnavich, P.M., & Koester, D. 1998, MNRAS, 298, 207.

Camillo, F., Lorimer, D.R., Freire, P., Lyne, A.G., & Manchester, R.N. 2000, ApJ, 535, 975.

Chan, K.L. & Chau, W.Y. 1979, ApJ, 233, 950.

D'Amico, N., Lyne, A. G., Manchester, R. N., Possenti, A., & Camilo, F. 2001, ApJ, 548, L171.

D'Antona, F., Mazzitelli, I., & Ritter, H. 1989, A&A, 225, 391.

Dewi, J.D.M. & Tauris, T.M. 2000, A&A, 360, 1043.

Dorman, B., Nelson, L.A., & Chau, W.Y. 1989, ApJ, 342, 1003.

Driebe, T., Schonberner, D., Blocker, T., & Herwig, F. 1998, A&A, 339, 123 [DSBH].

Eggleton, P.P. 1983, ApJ, 268, 368.

Ergma, E. & Sarna, M.J. 1996, MNRAS, 280, 1000.

Ergma, E., Sarna, M.J., & Antipova, J. 1998, MNRAS, 300, 352.

Fruchter, A. S., Stinebring, D. R., & Taylor, J. H. 1988, Nature, 333, 237.

Hameury, J.M., King, A.R., Lasota, J.P., & Ritter, H. 1988, MNRAS, 231, 535.

Hansen B.M.S. & Phinney E.S. 1998a, MNRAS, 294, 557 [HPa].

Hansen B.M.S. & Phinney E.S. 1998b, MNRAS, 294, 569 [HPb].

Howell, S. B., Nelson, L. A., & Rappaport, S. 2001, ApJ, 550, 897.

Hubbard, W. B. & Lampe, M. 1969, ApJS, 18, 163.

Iben I. Jr. & Tutukov A.V. 1986, ApJ, 311, 742 [IT].

Iglesias, C. A. & Rogers, F. J. 1996, ApJ 464, 943.

Itoh, N., Adachi, T., Nakagawa, M., Kohyama, Y., & Munakata, H. 1990, ApJ, 339, 354.

Johnston, S., Lorimer, D.R., Harrison, P.A., Bailes, M., Lyne, A.G., Bell, J.F., Kaspi, V.M., Manchester, R.N., D'Amico, N., Nicastro, L. & Jin S. 1993, Nature, 361, 613.

Joss, P. C. & Rappaport, S., 1976, ApJ, 208, L71.

Kalogera, V. & Webbink, R.F. 1998, ApJ, 493, 351.

Kaspi, V.M., Taylor, J.H., & Ryba, M.F. 1994, ApJ, 428, 713.

Kippenhahn R. & Weigert A., 1967, Z. Astrophys. 65, 251.

Kippenhahn R. & Weigert A., 1990, in *Stellar Structure and Evolution*, Astronomy & Astrophysics Library Series, (Berlin: Springer-Verlag).

Kolb, U., King, A., & Ritter, H. 1998, MNRAS, 298, L29.

Landau, L.D. & Lifshitz, E.M. 1962, *The Classical Theory of Fields*, (Oxford: Pergamon).

Livio, M. & Soker, N. 1988, ApJ, 329, 764.

Lorimer, D.R., Lyne, A.G., Festin, L., & Nicastro, L. 1995, Nature, 376, 393.

Magni, G. & Mazzitelli, I. 1979, A&A, 72, 134.

Maxted, P.F.L., Marsh, T.R., & Moran, C.K.J. 2002, MNRAS, 332, 745.

Meyer, F., & Meyer-Hofmeister, E. 1979, A&A, 78, 167.

Nelson, L.A., Chau, W.Y., & Rosenblum, A. 1985, ApJ, 299, 658.

Nelson, L.A. and Davis, A. 2000, "On the Companions of Binary Millisecond Pulsars" in *Proceedings of the Warner Symposium*, eds., P. Charles, A. King, D. O'Donoghue, New Astronomy Reviews, 44, 99 [ND].

Nelson, L.A. 2004a, (in preparation).

Nelson, L.A. 2004b, in *Binary Radio Pulsars*, eds. F. Rasio and I. Stairs, ASP Conference Series, (in press).

Nelson, L.A. & Dubeau, E. 2004a, (in preparation).

Nelson, L.A. & Dubeau, E. 2004b, (in preparation).

Nelson, L.A., Joss, P.C., & Rappaport, S. 1989, IAU Colloq. 114, *White Dwarfs*, ed. G. Wegner (Berlin: Springer), 469.

Nelson, L.A., MacCannell, K.A., & Davis, A. 2001 in *Evolution of Binary and Multiple Star Systems*, eds. Ph. Podsiadlowski, S. Rappaport, A.R. King, F. D'Antona and L. Burderi, ASP Conference Series, 229, 223.

Nelson, L.A. & Rappaport, S. 2003, ApJ, 598, 431 [NR].

Nelson, L.A. & Rappaport, S. 2004, (in preparation).

Nelson, L.A., Rappaport, S.A., & Joss, P.C. 1986, ApJ, 304, 231 [NRJ].

Nice, D., Splaver, E. M., & Stairs, I. H. 2003, in *Radio Pulsars*, eds. M. Bailes, D. J. Nice, & S. E. Thorsett, ASP Conference Series, 302, 75.

Paczyński, B., 1971, ARAA, 9, 183.

Paczyński, B., & Sienkiewicz, R. 1981, ApJ, 248, 27.

Pfahl, E.D., Rappaport, S., & Podsiadlowski, Ph. 2003, ApJ, 597, 1036.

Podsiadlowski, P., Han, Z., & Rappaport, S. 2003, MNRAS, 340, 1214.

Podsiadlowski, P., Rappaport, S., & Pfahl, E.D. 2002, ApJ, 565, 1107 [PRP].

Prialnik, D., & Kovetz, A. 1995, ApJ, 445, 789.

Pylyser, E. & Savonije, G.J. 1988, A&A, 191, 57 [PS].

Pylyser, E. & Savonije, G.J. 1989, A&A, 208, 52.

Rappaport, S., Joss, P. C., & Lewis, W. 1987, ApJ, 319, 180.

Rappaport, S., Joss, P.C., & Webbink, R.F. 1982, ApJ, 254, 616 [RJW].

Rappaport S., Podsiadlowski Ph., Joss P.C., Di Stefano R., & Han Z. 1995, MNRAS 273, 731.

Rappaport, S., Verbunt, F., & Joss, P. C. 1983, ApJ, 275, 713 [RVJ].

Rasio, F. A., Pfahl, E. D., & Rappaport, S. 2000, ApJ, 532, L47.

Reimers, D. 1975 in *Problems in Stellar Atmospheres and Envelopes*, eds. B. Baschek, W.H. Kegel, G. Traving (New York: Springer-Verlag), p229.

Sandhu, J.S., Bailes, M., Manchester, R.N., Navarro, J., Kulkarni, S.R., & Anderson, S.B. 1997, ApJ, 478, L95.

Sarna, M. J., Ergma, E., & Gerskevits-Antipova, J. 2000, MNRAS, 316, 84 [SEG].

Saumon, D., Chabrier, G., & Van Horn, H. M. 1995, ApJS, 99, 713.

Schenker, K., Kolb, U., & Ritter, H. 1998, MNRAS, 297, 633.

Segelstein, D.J., Rawley, L.A., Stinebring, D.R., Fruchter, A.S., & Taylor, J.H. 1986, Nature, 322, 714.

Spruit, H. C., & Ritter, H. 1983, A&A, 124, 267.

Taam, R.E., Bodenheimer, P., & Ostriker, J. P. 1978, ApJ, 222, 269.

Tauris, T.M. & Savonije, G.J. 1999, A&A, 350, 928 [TS].

Tauris, T.M., van den Heuvel, E.P.J., & Savonije, G.J. 2000, ApJ, 530, L93.

Thorsett, S.E. & Chakrabarty, D. 1999, ApJ, 512, 288.

Tutukov, A.V., Fedorova, A.V., Ergma E., & Yungelson, L.R. 1985, Soviet Astron. Lett., 11, 123.

van Kerkwijk, M.H., Bell, J.F., Kaspi, V.M., Kulkarni, S.R. 2000, ApJ, 530, L37.

van Kerkwijk, M.H., Bergeron, P., & Kulkarni, S.R. 1996, ApJ, 467, L89.

van Straten, W., Bailes, M., Britton, M., Kulkarni, S.R., Anderson, S.B., Manchester, R.N., & Sarkissian, J. 2001, Nature, 412, 158.

Verbunt, F. & Zwaan, C. 1981, A&A, 100, L7.

Warner, B. 1995, in *Cataclysmic Variable Stars*, Cambridge Astrophysics Series, (New York: Cambridge University Press).

Watson, M.G., King, A.R., & Osborne, J. 1985, MNRAS, 212, 917.

Webbink, R.F. 1975, MNRAS, 171, 555.

Webbink, R. 1992, in *X-Ray Binaries and Recycled Pulsars*, ed. E.P.J. van den Heuvel and S. Rappaport (Dordrecht: Kluwer), 269.

Webbink, R.F., Rappaport, S., & Savonije, G.J. 1983, ApJ, 270, 678.

Willson, L.A. 2000, ARAA, 38, 573.

Willems, B. & Kolb, U. 2002, MNRAS, 337, 1004.

Yungelson, L.R., Nelemans, G., Portegies Zwart, S.F., & Verbunt, F. 2001 in *The Influence of Binaries on Stellar Population Studies*, ed. D. Vanbeveren, (Kluwer Academic Publishing), 339.

Zaplosky, H.S. & Salpeter E.E. 1969, ApJ, 158, 809.

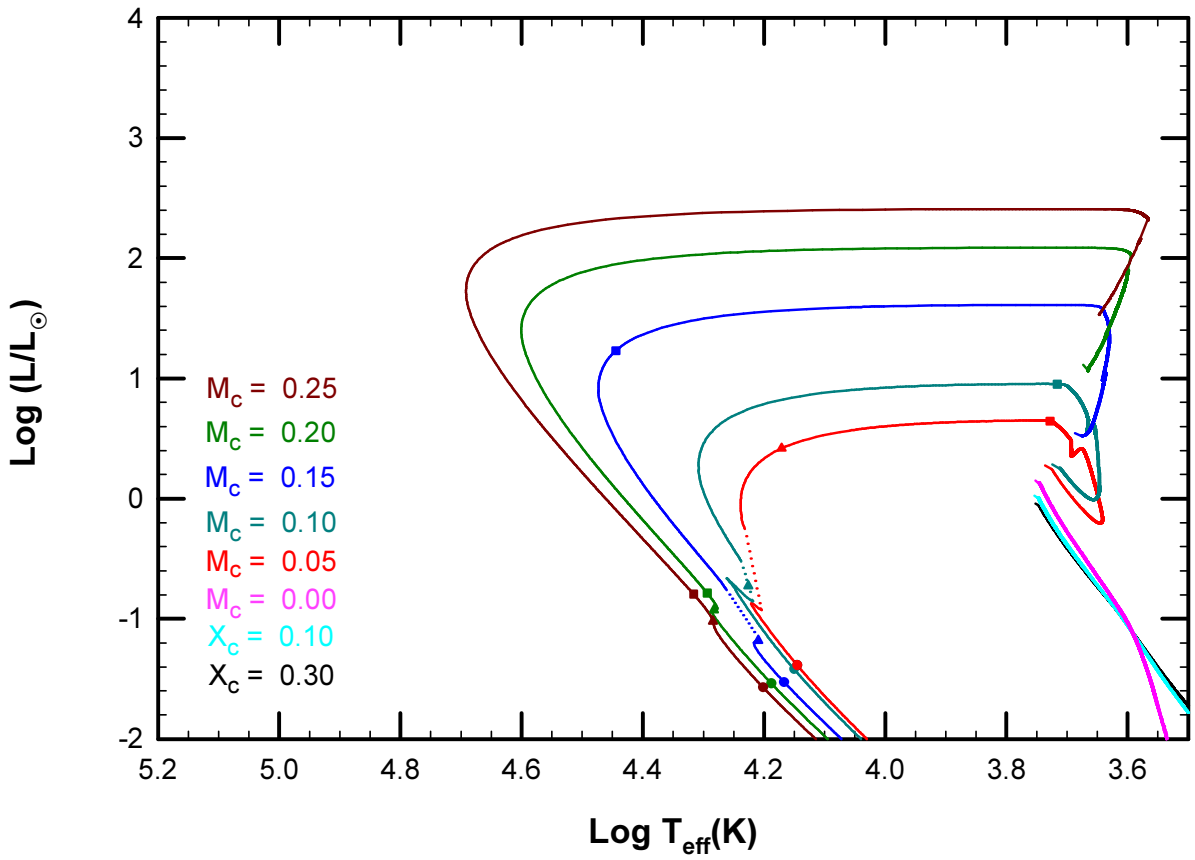

Fig. 1.— Evolutionary tracks of donors in interacting binaries plotted on the HR diagram. For each track, the initial mass of the donor is $1.0M_{\odot}$, its metallicity is $Z = 0.02$, and the mass of the compact companion is $1.4M_{\odot}$. The numbers adjacent to each track denote the initial core masses ($m_{c,0}$). For those systems that have not formed a core, the initial central H-abundance ($X_{c,0}$) is labeled. [In the electronic edition: The symbols X_c and M_c denote the values of the central hydrogen content and the helium core mass (in solar masses) of the donor at the onset of mass transfer, respectively.] Note that $M_c = 0.00$ is equivalent to $X_c = 0$. Donors that experience vigorous hydrogen shell flashes have their tracks interrupted by dotted lines. The endpoints of the dotted lines denote the location of the beginning and ending of the shell flashes. The actual shell-flash evolution is omitted for reasons of clarity and is investigated in more detail (see Figures 12 & 19). The age of the donor after its detachment from the Roche lobe (near the RGB) is denoted by squares (10^7 yr), triangles (10^8 yr), and dots (10^9 yr).

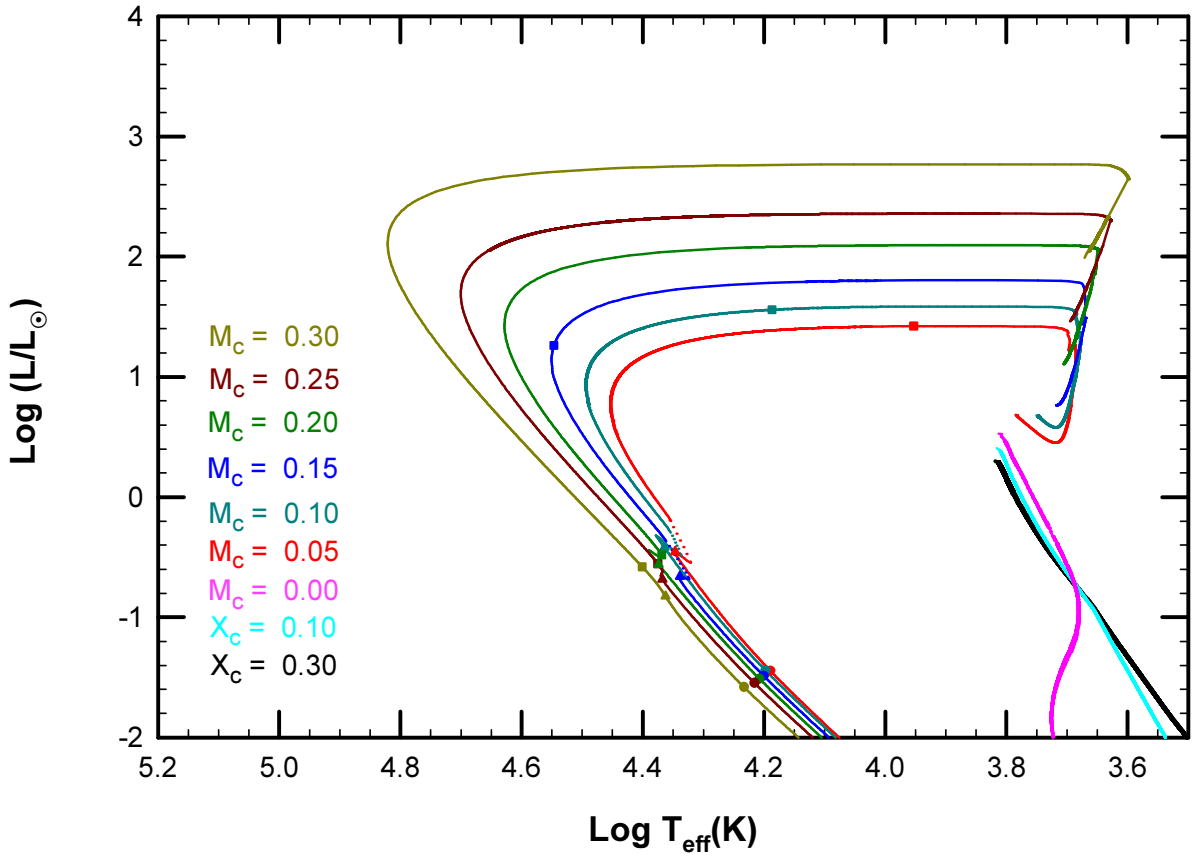

Fig. 2.— Evolutionary tracks of an initially $1.0M_{\odot}$ donor with a metallicity of $Z = 0.004$ plotted on the HR diagram. The mass of the compact companion is $1.4M_{\odot}$. The labeling follows the same format as described in Figure 1.

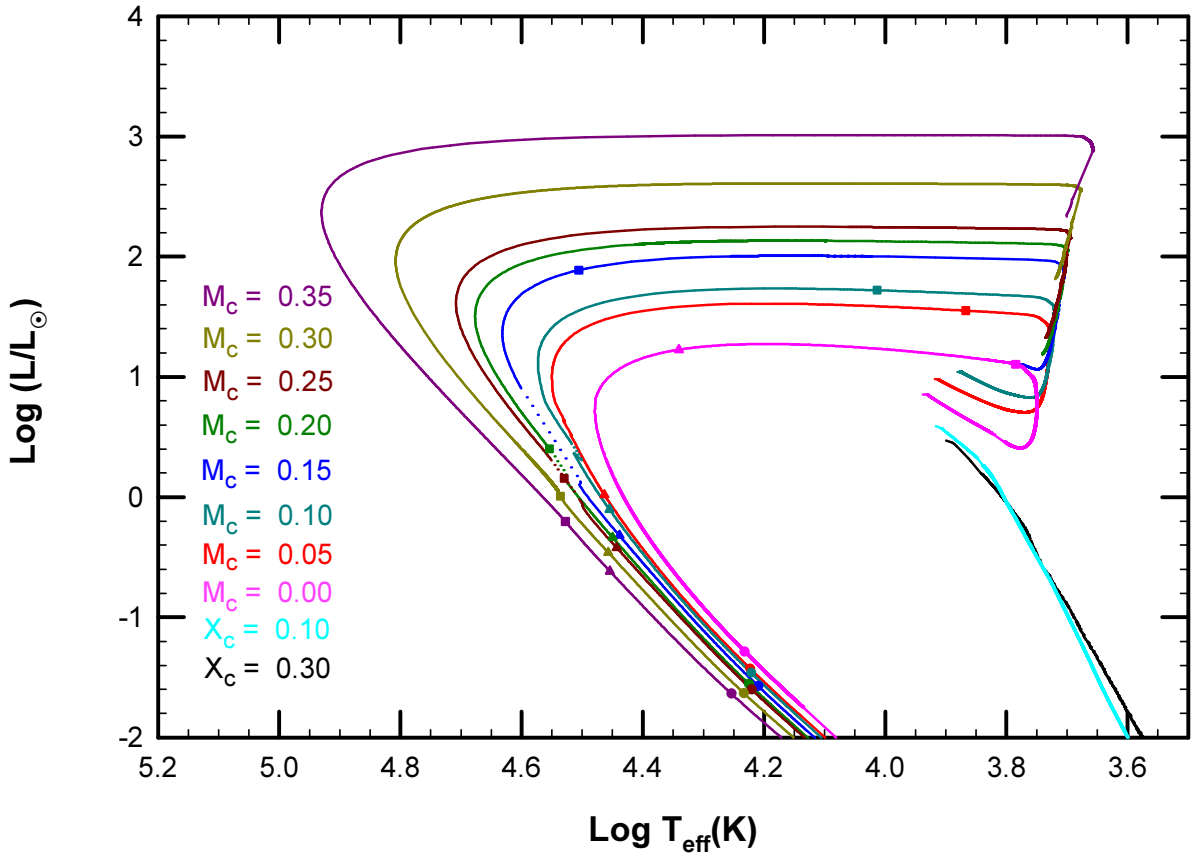

Fig. 3.— Evolutionary tracks of an initially $1.0M_{\odot}$ donor with a metallicity of $Z = 0.0001$ plotted on the HR diagram. The mass of the compact companion is $1.4M_{\odot}$. The labeling follows the same format as described in Figure 1.

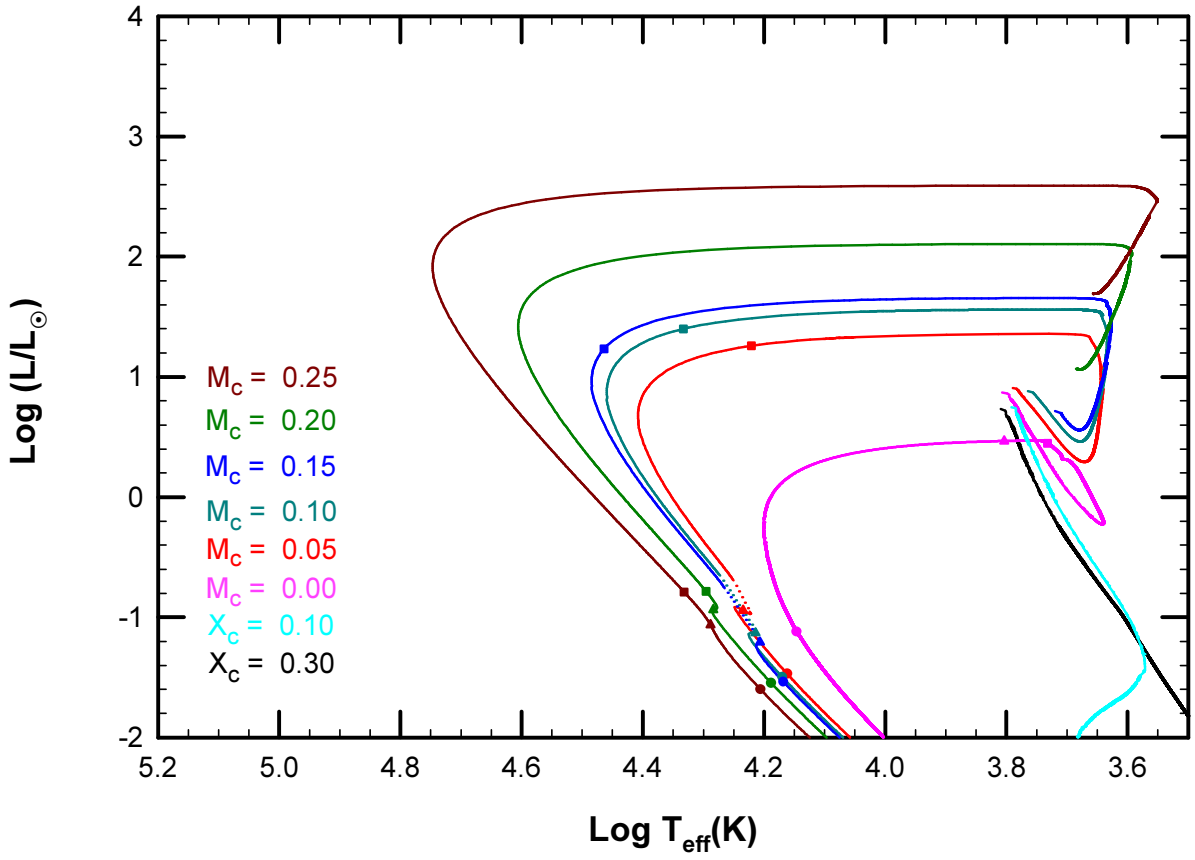

Fig. 4.— Evolutionary tracks of an initially $1.5M_\odot$ donor with a metallicity of $Z = 0.02$ plotted on the HR diagram. The mass of the compact companion is $1.4M_\odot$. The labeling follows the same format as described in Figure 1.

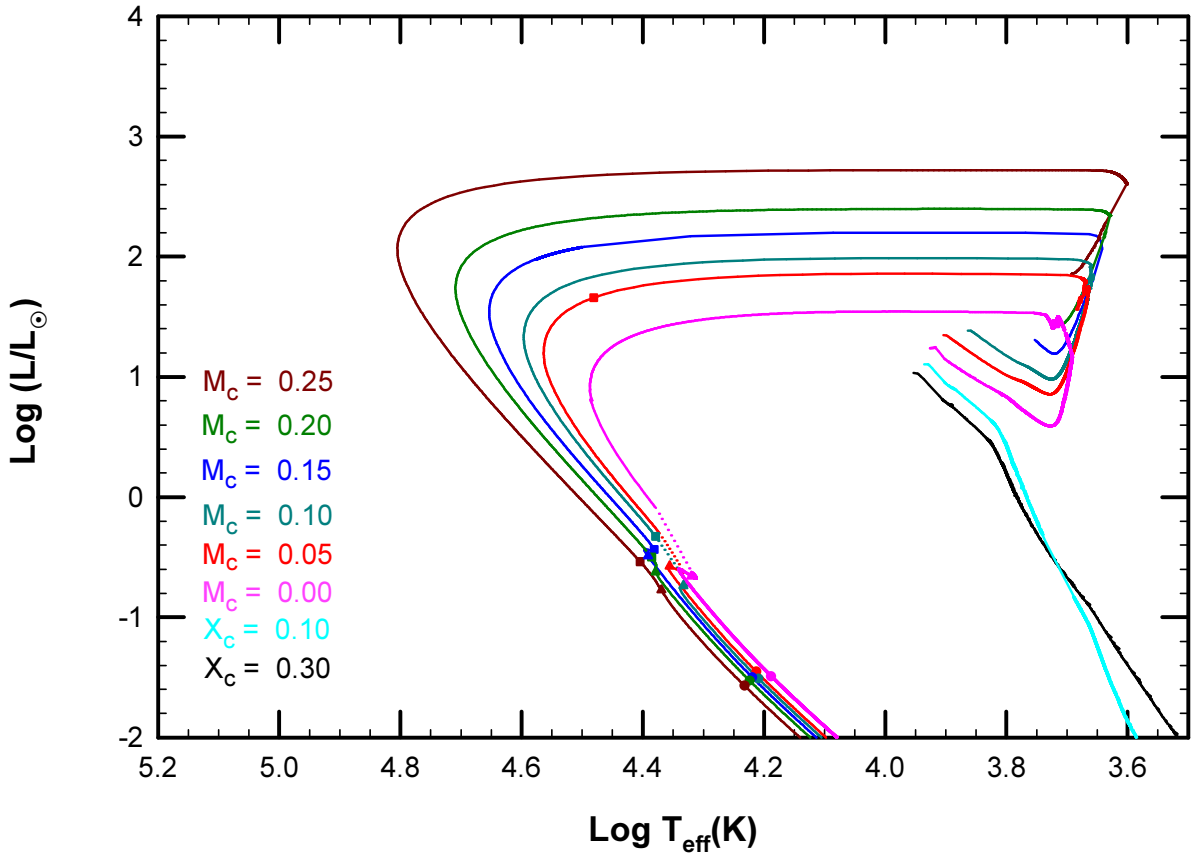

Fig. 5.— Evolutionary tracks of an initially $1.5M_{\odot}$ donor with a metallicity of $Z = 0.004$ plotted on the HR diagram. The mass of the compact companion is $1.4M_{\odot}$. The labeling follows the same format as described in Figure 1.

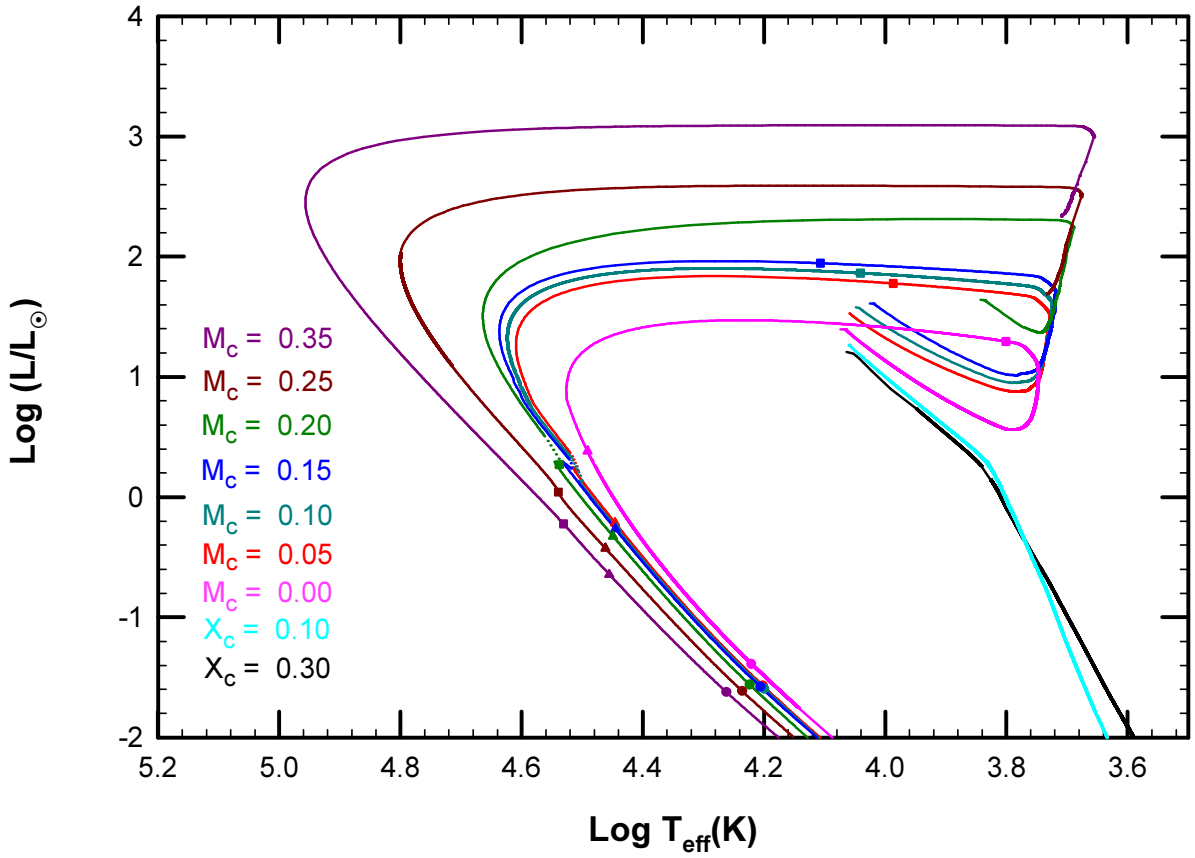

Fig. 6.— Evolutionary tracks of an initially $1.5M_\odot$ donor with a metallicity of $Z = 0.0001$ plotted on the HR diagram. The mass of the compact companion is $1.4M_\odot$. The labeling follows the same format as described in Figure 1.

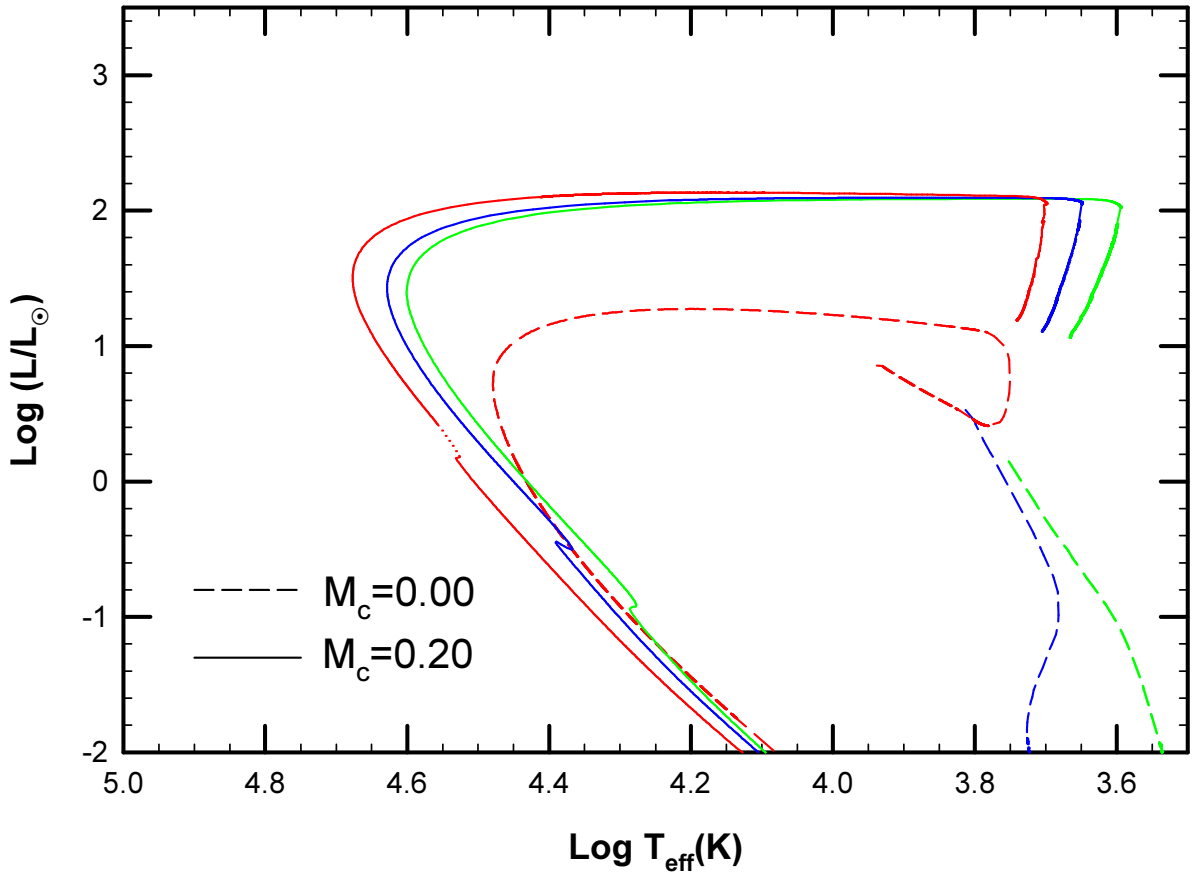

Fig. 7.— Evolution of a $1.0M_{\odot}$ donor losing mass to a $1.4M_{\odot}$ accretor in the HR diagram. Two separate cases are considered, one for which the original value of $m_c = 0$ (gray curves) and the other corresponding to initial core masses of $0.20M_{\odot}$ (black curves). The solid, dashed, and dotted curves correspond to metallicities of $Z = 0.0001$, 0.004, and 0.02, respectively. [In the electronic edition: Two separate cases are considered, one for which the original value of $m_c = 0$ (dashed lines) and the other corresponding to initial core masses of $0.20M_{\odot}$ (solid lines). The red, blue, and black curves correspond to metallicities of $Z = 0.0001$, 0.004, and 0.02, respectively.]

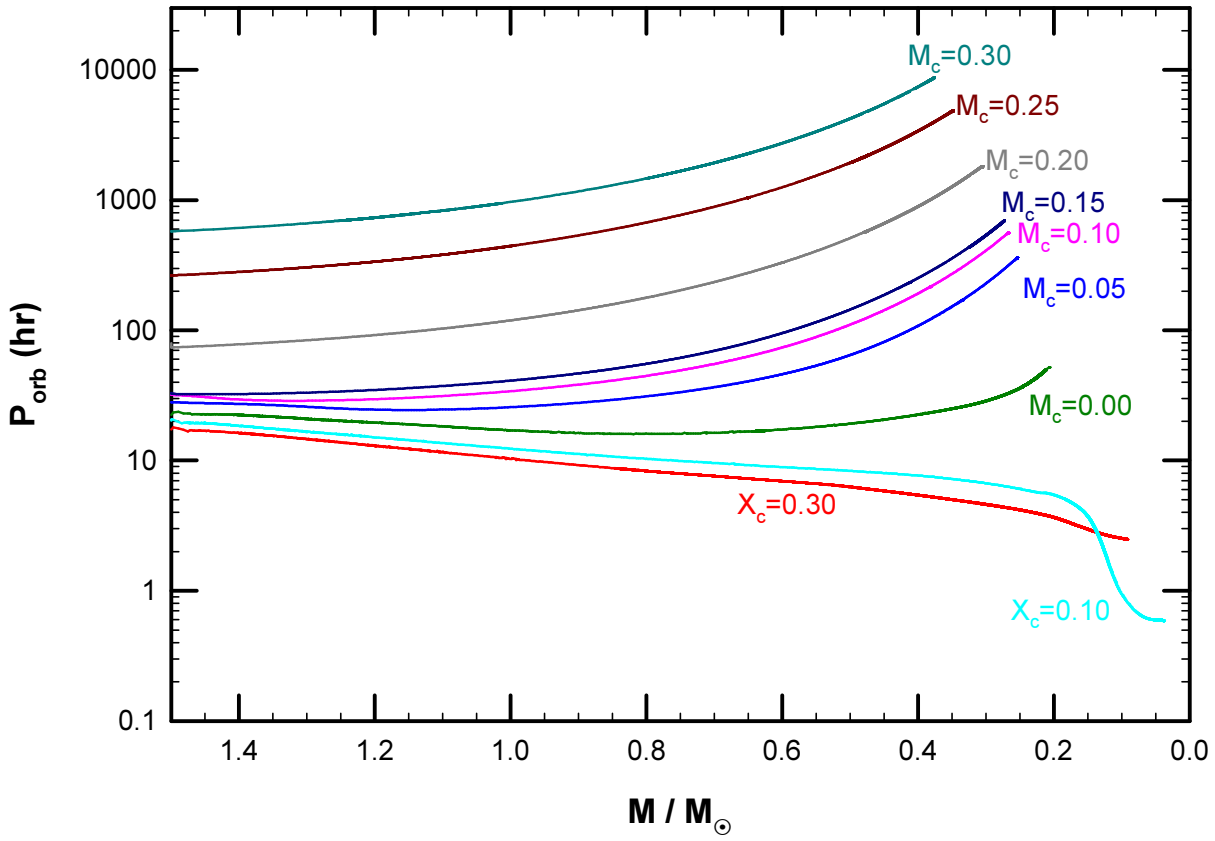

Fig. 8.— Orbital period evolution plotted versus $M_2/M_\odot$ for an initial donor mass of $1.5M_\odot$, with a metallicity of $Z = 0.02$. For all tracks the mass of the accretor is $1.4M_\odot$. The symbols X_c and M_c denote the values of the central hydrogen content and the helium core mass (in solar masses) of the donor at the onset of mass transfer, respectively. A very sharp bifurcation is seen for initial values of P_{orb} of $\lesssim 20$ hours.

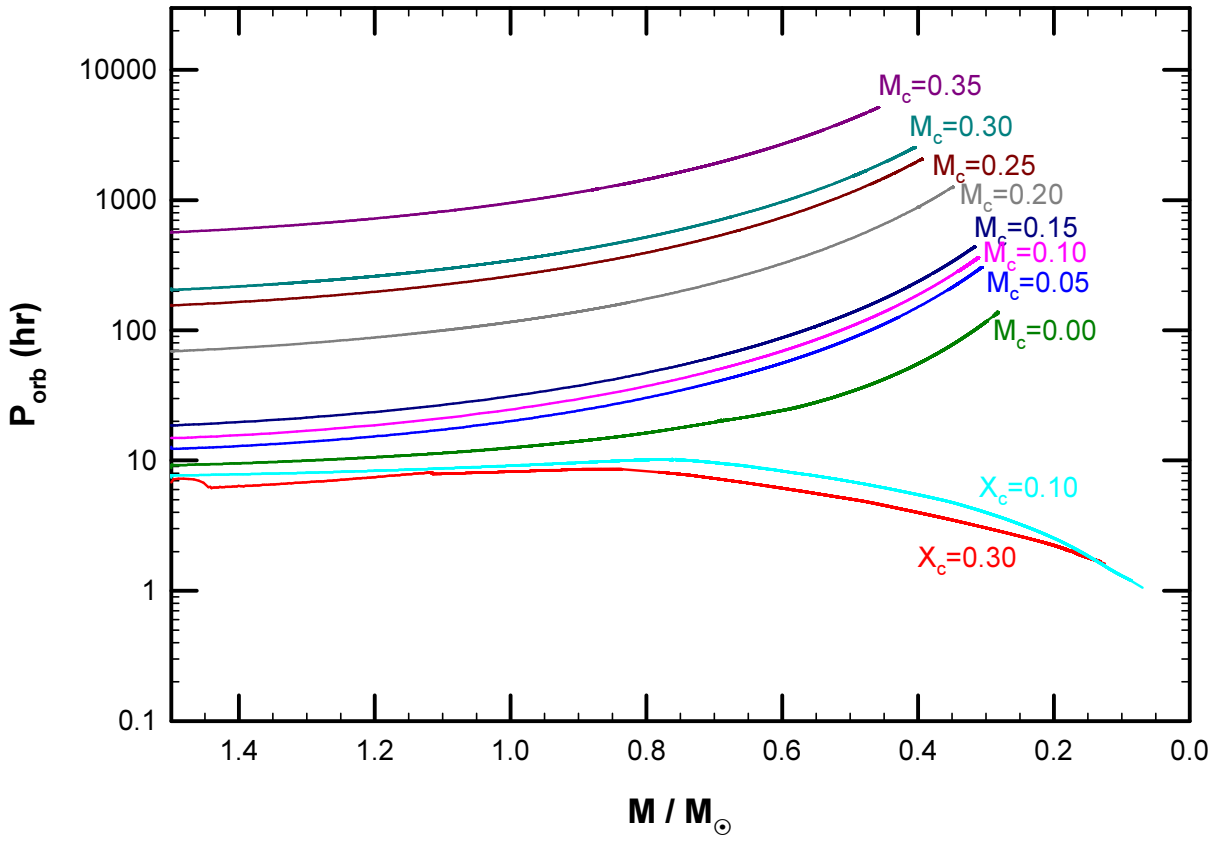

Fig. 9.— Orbital period evolution plotted versus $M_2/M_\odot$ for an initial donor mass of $1.5M_\odot$ with a metallicity of $Z = 0.0001$. For all tracks the mass of the accretor is $1.4M_\odot$. The symbols X_c and M_c denote the values of the central hydrogen content and the helium core mass (in solar masses) of the donor at the onset of mass transfer, respectively. A very sharp bifurcation is seen for initial P_{orb}'s of $\lesssim 8$ hours.

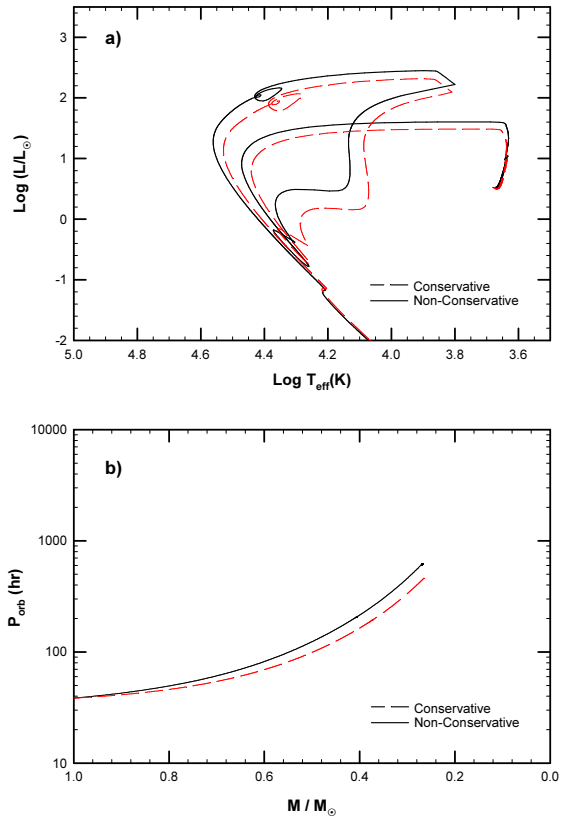

Fig. 10.— Evolution of binaries containing donors with an initial mass of $1.0M_\odot$ and having a solar metallicity ($Z = 0.02$). The initial core mass of each donor is $0.25M_\odot$ and it is transferring mass to a $1.4M_\odot$ accretor. Its evolution in the HR diagram is shown in panel a). The solid curve corresponds to the non-conservative case ($\beta = 0$) and the dashed curve corresponds to the conservative case ($\beta = 1$). Note that the donor experiences one shell flash cycle (see §3.2 for more details on this phase of evolution). In panel b) the corresponding evolution of the orbital periods is plotted versus $M_2/M_\odot$ for both the conservative and non-conservative cases.

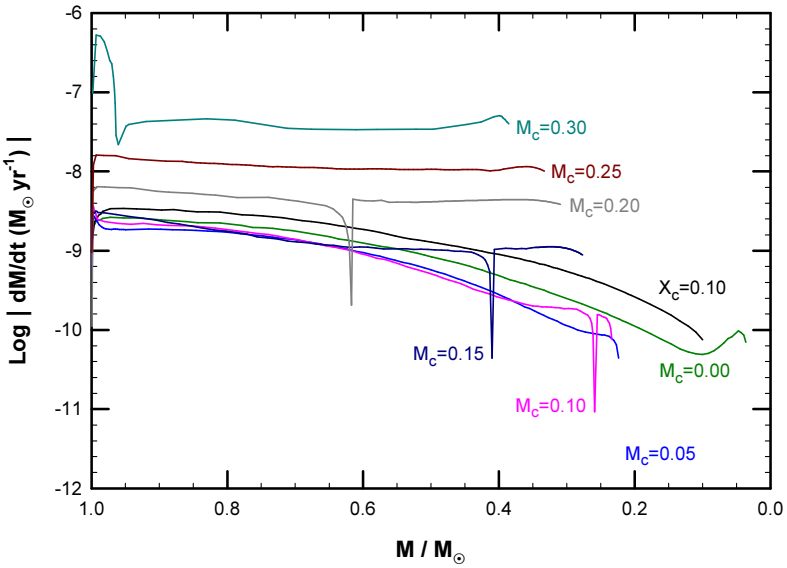

Fig. 11.— Evolution of the log of the secular (averaged) mass-transfer rate from the donor to the accretor (in units of $M_\odot$ yr^{-1}) as a function of the mass of the donor (in solar units). For all tracks the initial mass of the donor is $1.0M_\odot$, its metallicity is $Z = 0.02$, and the mass of the accretor is $1.4M_\odot$. The symbols X_c and M_c denote the values of the central hydrogen content and the helium core mass (in solar masses) of the donor at the onset of mass transfer, respectively. Some tracks exhibit temporary mass cessations as they are ascending the RGB (these can be seen as sharp downward spikes). For cases that ultimately produced HeDD's, the endpoints of those tracks correspond to the point where mass transfer ceases permanently. For the other cases, the endpoints simply reflect the value of M_2 at which the computation was halted.

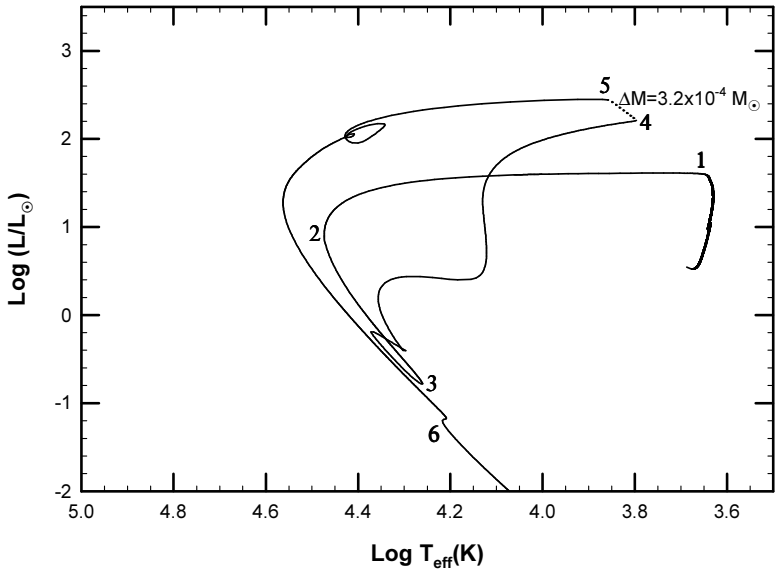

Fig. 12.— Evolution of a donor with an initial mass of $1.0M_{\odot}$ and a solar metallicity ($Z = 0.02$) that undergoes a shell flash. The initial core mass of the donor is $0.15M_{\odot}$ and it is losing mass to a $1.4M_{\odot}$ accretor. Important junctures during the shell flash are indicated by numbers labeled from 1 to 6. The first major thermal pulse occurs at point 3. When the donor refills its Roche lobe at point 4, mass transfer recommences. This mass-loss phase of the evolution occurs until points 5 and is denoted by a dotted line. The amount of mass that is lost from the donor (ΔM) is given in solar units.

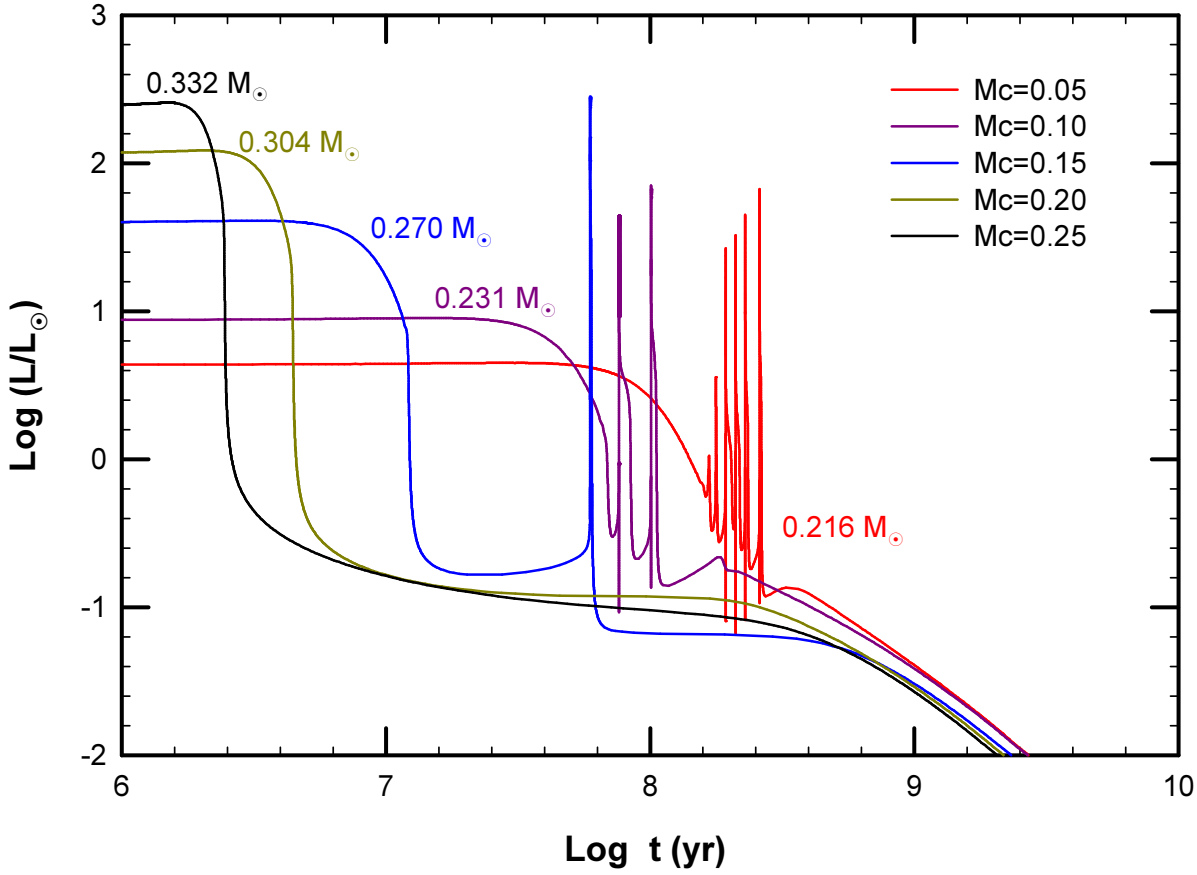

Fig. 13.— Temporal evolution of the luminosity of the donor (L_2) as a function of the time elapsed since the initial detachment of the donor from its Roche lobe near the RGB. For each curve, the initial mass of the donor is $1.0M_{\odot}$ with a metallicity of ($Z = 0.02$). The final HeDD masses corresponding to each curve are listed in solar units. Each curve corresponds to a different initial core mass ($m_{c,o}$; labeled as Mc) and the accretor is a $1.4M_{\odot}$ compact object. Vigorous shell flashes cause the luminosity of the donor to increase by several orders of magnitude on a short timescale and thus are seen as vertical spikes in the diagram.

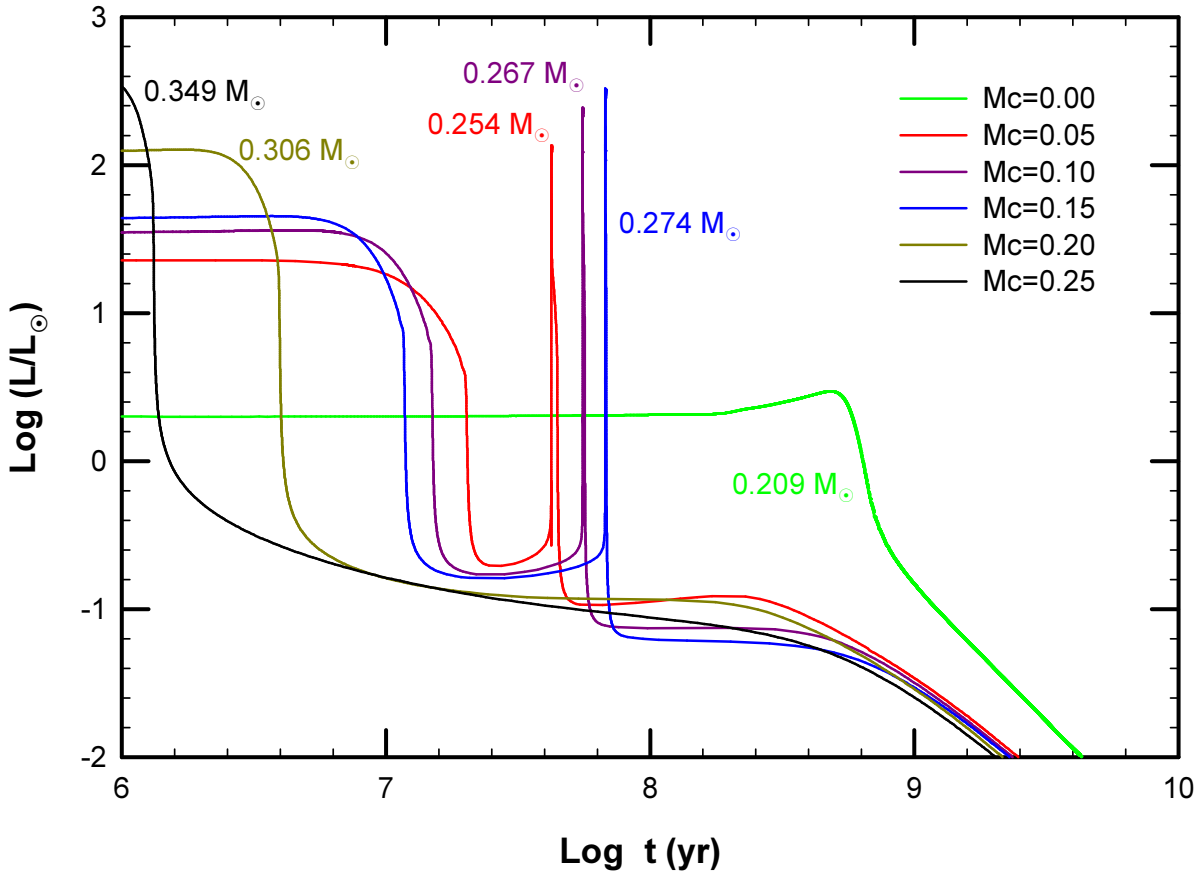

Fig. 14.— Temporal evolution of the luminosity of the donor (L_2) as a function of the time elapsed since the initial detachment of the donor from its Roche lobe near the RGB. For each curve, the initial mass of the donor is $1.5M_{\odot}$ and its metallicity is ($Z = 0.02$). The final HeDD masses corresponding to each curve are listed in solar units. Each curve corresponds to a different initial value of core mass (at the onset of mass transfer) and the accretor was a $1.4M_{\odot}$ compact object. For some of the tracks, vigorous shell flashes cause the luminosity of the donor to increase by several orders of magnitude on a short timescale thus producing almost vertical spikes.

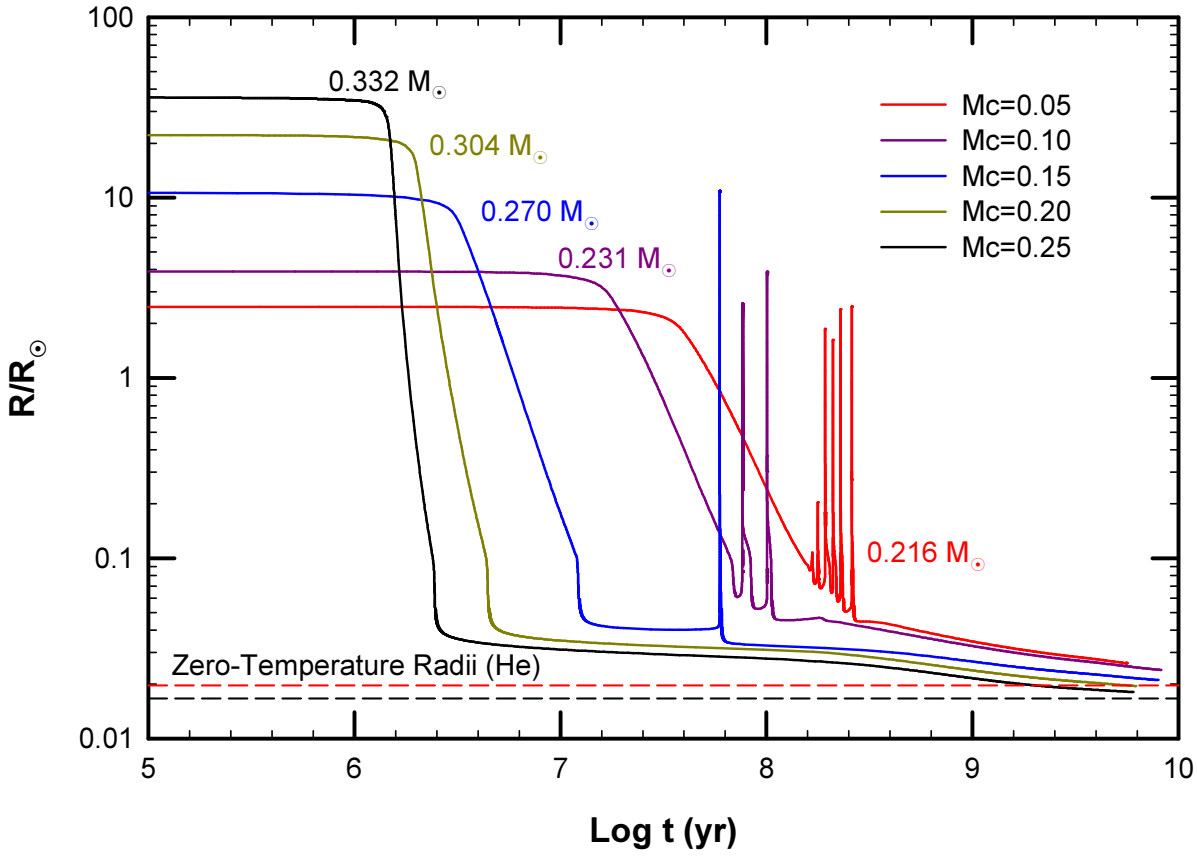

Fig. 15.— Temporal evolution of the radius of the donor (R_2) as a function of the time elapsed since the initial detachment of the donor from its Roche lobe near the RGB. For each curve, the initial mass of the donor was $1.0M_\odot$ and its metallicity was $Z = 0.02$ (the accretor is a $1.4M_\odot$ compact object). The values of the initial core mass (m_c in units of solar masses) are listed in the figure. Vigorous shell flashes cause the radius of the donor to increase on a short timescale and thus produce the almost vertical spikes seen in the figure. The zero-temperature radii of the lowest and highest mass models are denoted by dotted lines (values calculated assuming a pure He composition). [In the electronic edition: The zero-temperature radii of the lowest and highest mass models are denoted by dashed lines (values calculated assuming a pure He composition).]

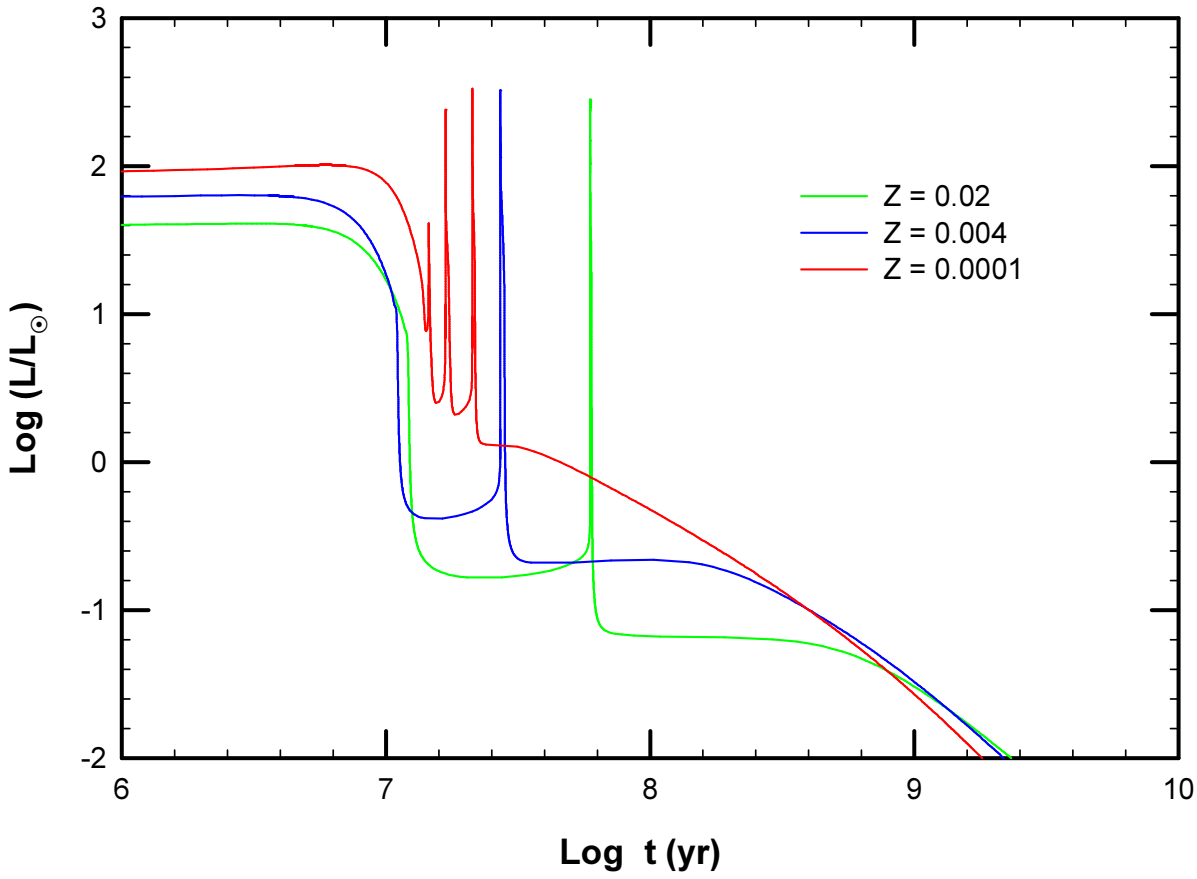

Fig. 16.— Temporal evolution of the luminosity of the donor (L_2) as a function of the time elapsed since the initial detachment of the donor from its Roche lobe (after leaving the RGB). For each curve, the initial mass of the donor is $1.0M_{\odot}$ and its initial core mass is $0.15M_{\odot}$ and the accretor is a $1.4M_{\odot}$ compact object. The values of the metallicity (Z) are listed in the legend. Vigorous shell flashes cause the luminosity of the donor to increase by several orders of magnitude on a short timescale (nearly vertical spikes).

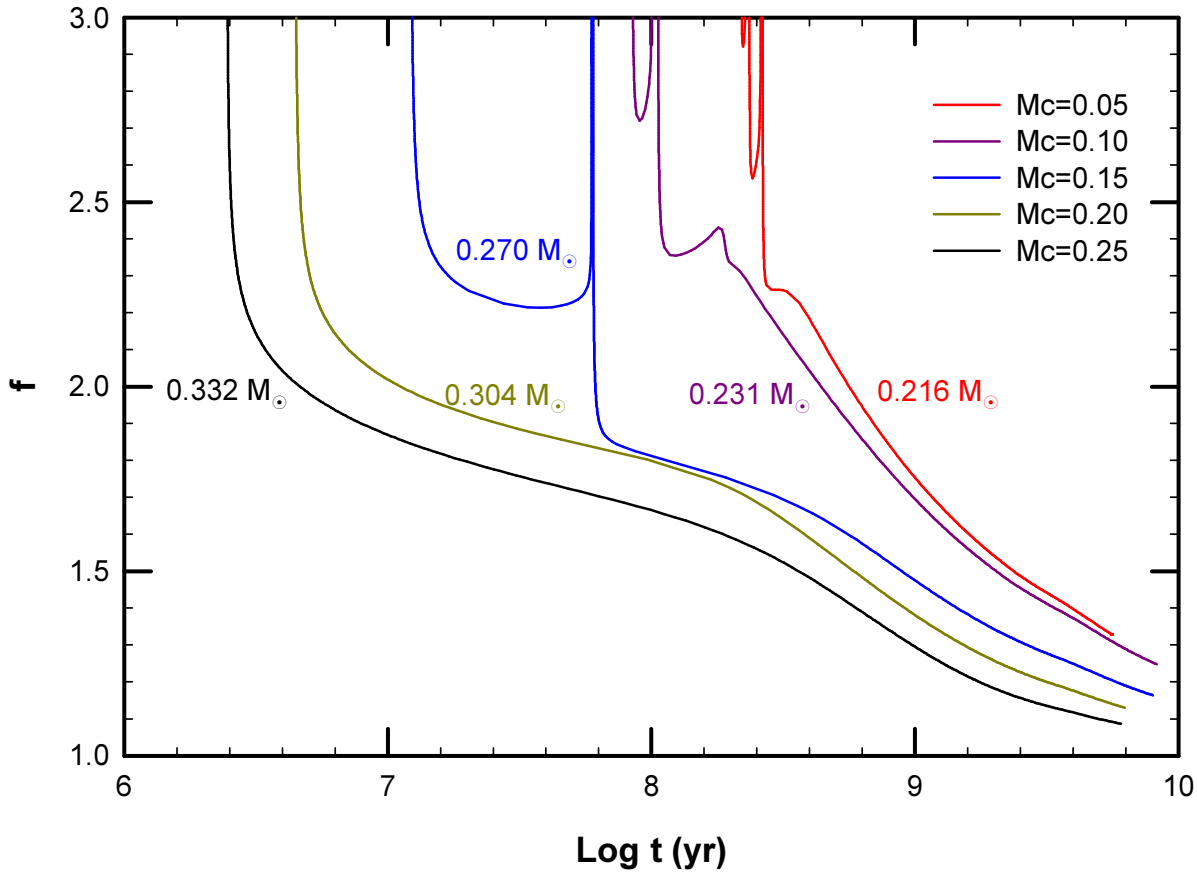

Fig. 17.— Cooling evolution of the donor expressed in terms of the thermal bloating factor f ($\equiv R_2/R_o$). R_o is the zero-temperature radius of a star of identical mass that is composed only of helium. Each curve is labeled with the final mass of the cooling dwarf. The initial core masses ($m_{c,0}$) labelled as Mc (in solar units) are shown in the legend. The initial masses of the donor ($Z = 0.02$) and accretor are 1.0 and 1.4 $M_\odot$, respectively.

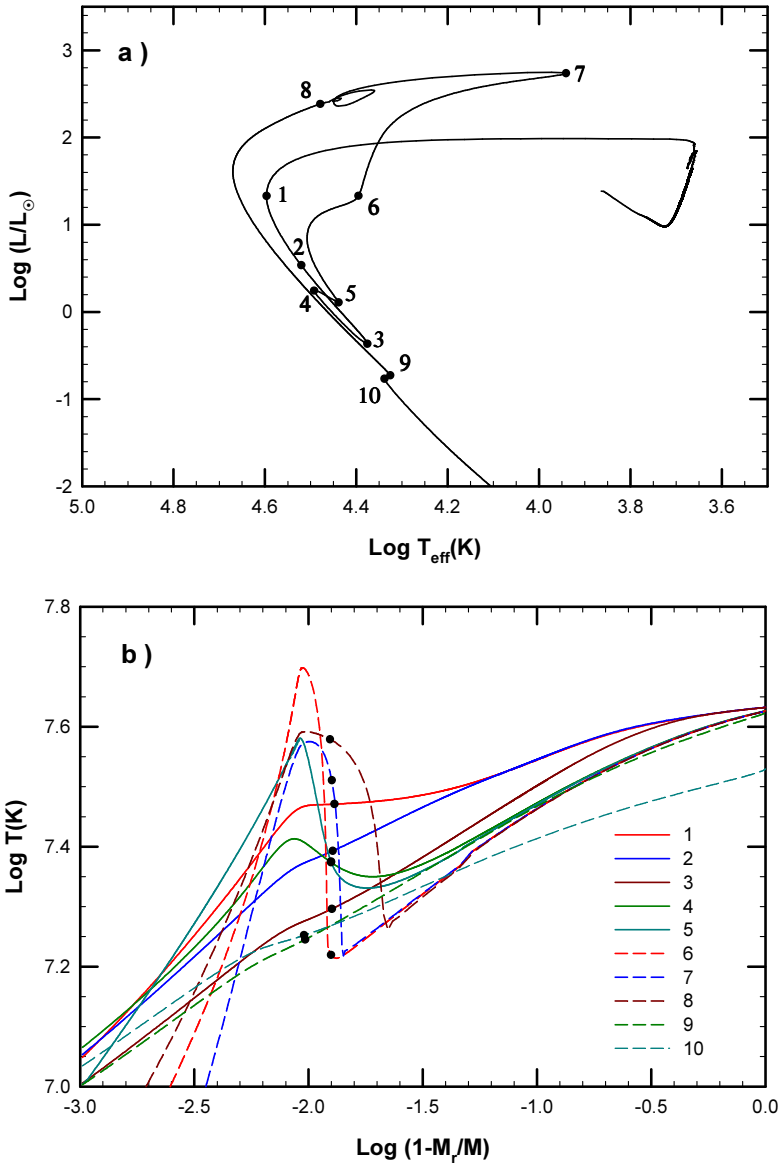

Fig. 18.— Evolution of a donor with an initial mass of $1.5M_\odot$ and a metallicity of $Z = 0.004$. The initial core mass of the donor is $0.10M_\odot$ and the accretor's mass is $1.4M_\odot$. Its evolution in the HR diagram is shown in panel a). Important junctures during the shell-flash phase are indicated by dots that are labeled by numbers from 1 through 10. The first major thermal pulse occurs at point 3. In panel b) the corresponding evolution of the temperature profile throughout the interior of the HeDD is shown. The log of T is plotted against the log of the mass fraction (i.e., $\log(1 - m_r/m)$ where m_r is the mass enclosed within a radius equal to r). The solid black dots in panel b) denote the approximate location of the boundary between the envelope and the He-rich core.

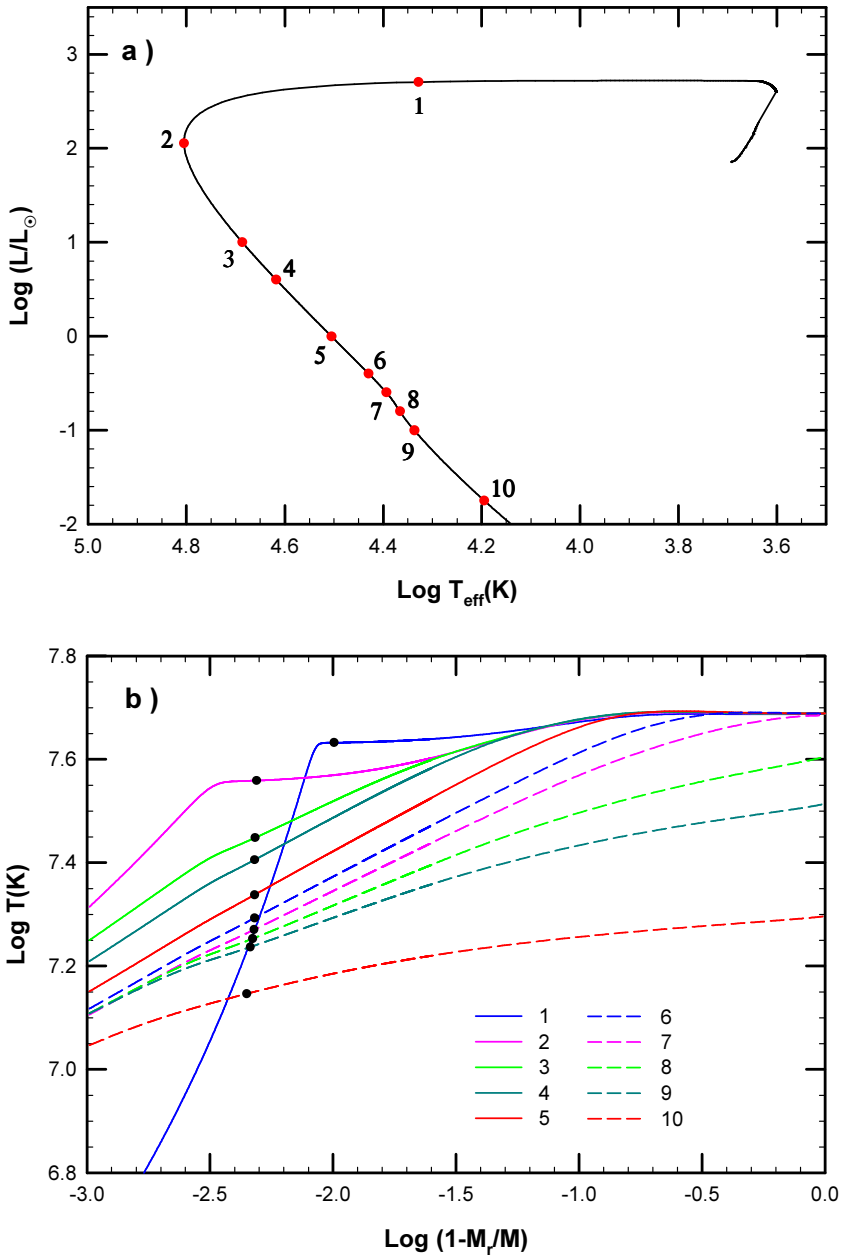

Fig. 19.— Evolution of a donor with an initial mass of $1.5M_\odot$ and a metallicity of $Z = 0.004$. The initial core mass of the donor is $0.25M_\odot$ and it is transferring mass to a $1.4M_\odot$ accretor. Its evolution in the HR diagram is shown in panel a). Important junctures during the shell flash are indicated by dots that are labeled by numbers 1 through 10. In panel b) the corresponding evolution of the temperature profile of the interior of the HeDD is shown. The log of T is plotted against the log of the mass fraction (i.e., $\log(1 - m_r/m)$ where m_r is the mass enclosed within a radius equal to r). The solid black dots in panel b) denote the approximate location of the boundary between the envelope and the He-rich core.

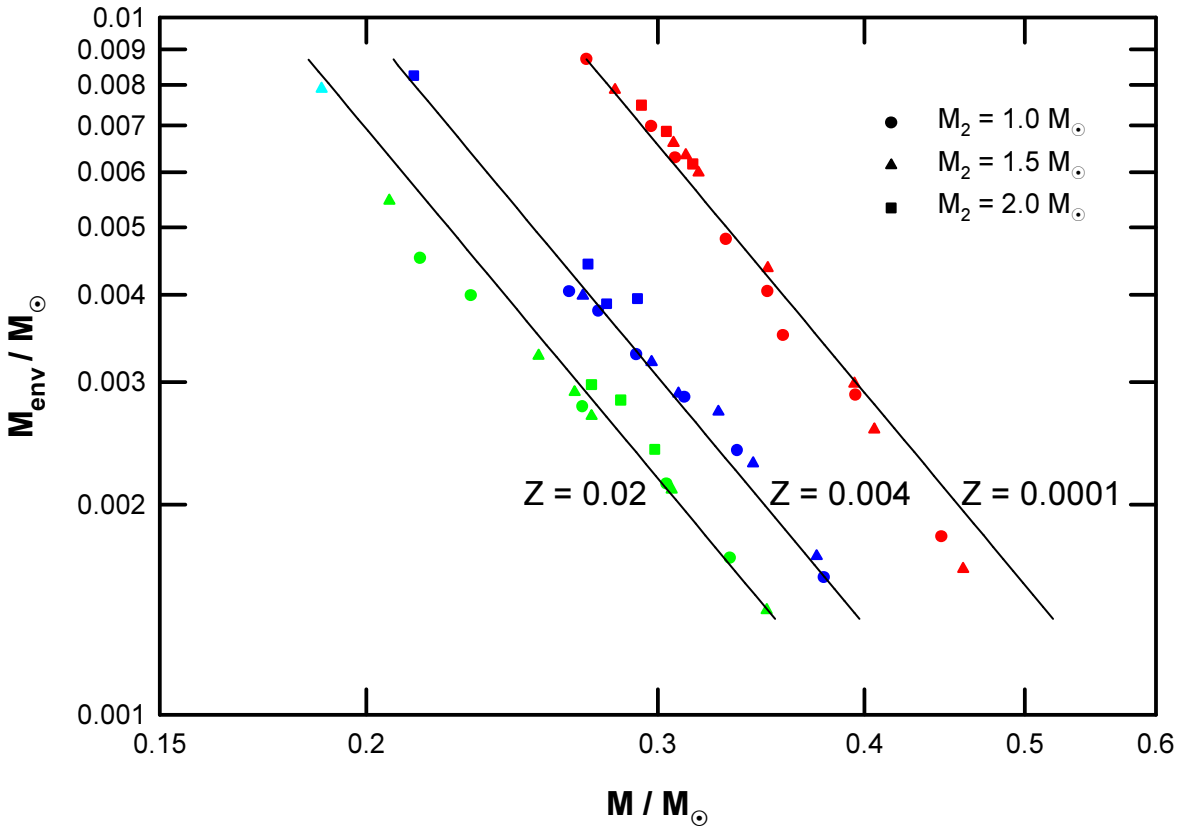

Fig. 20.— Dependence of the envelope mass (m_{env}) in units of solar masses on the final mass of the HeDD (determined at $\log(L/L_{\odot}) = -2$). The initial masses of the donors (at the onset of mass transfer) are denoted by circles, triangles, and squares as shown in the legend. The regression lines for the three metallicities are also shown. The various shades of gray correspond to different metallicities (Z=0.02 is black, Z=0.004 is light gray, Z=0.0001 is medium gray). [In the electronic edition: The various colors correspond to different metallicities (Z=0.02 is green, Z=0.004 is blue, Z=0.0001 is red).]

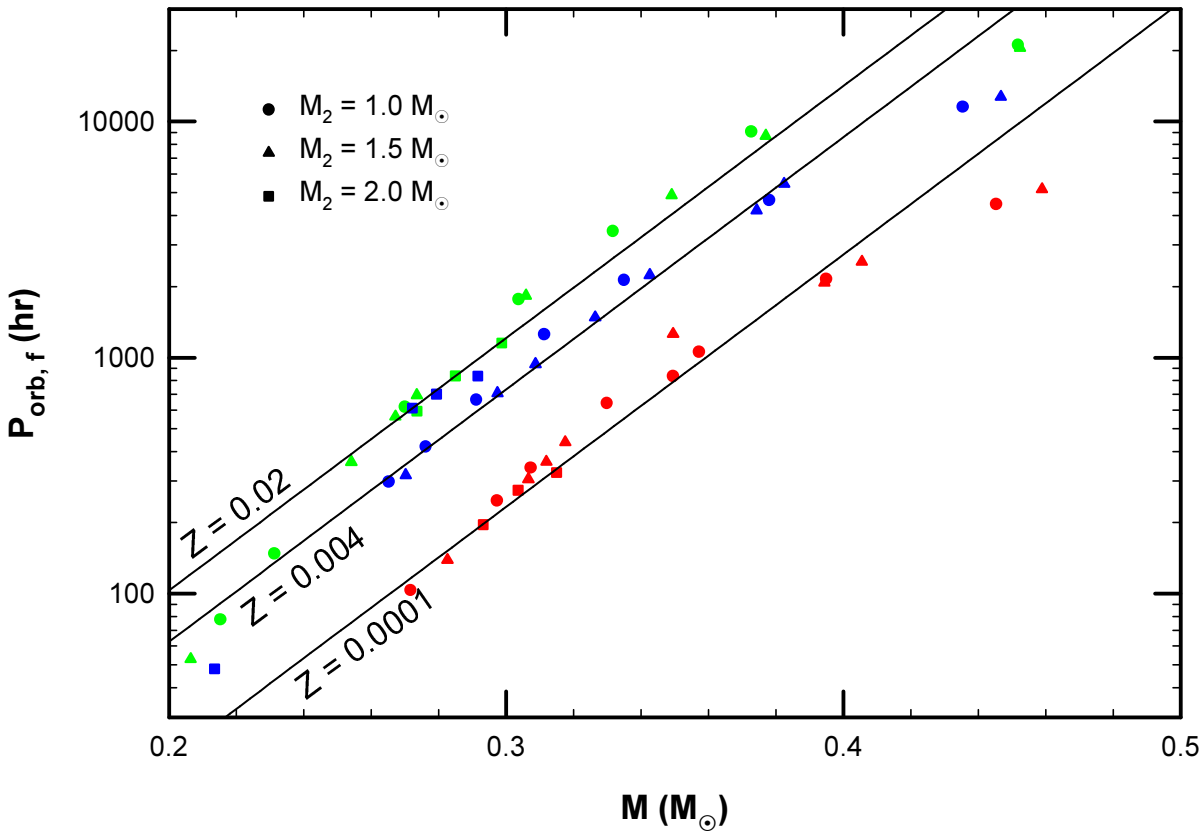

Fig. 21.— Dependence of the final orbital period ($P_{orb,f}$ in hours) on the final mass of the HeDD. The initial mass of the donors (at the onset of mass transfer) is denoted by circles, triangles, and squares as shown in the legend. The regression lines for the three metallicities are also shown. The various shades of gray correspond to different metallicities (Z=0.02 is black, Z=0.004 is light gray, Z=0.0001 is medium gray). [In the electronic edition: The various colors correspond to different metallicities (Z=0.02 is green, Z=0.004 is blue, Z=0.0001 is red).] The regression line fit must be used with caution for high-mass HeDD's ($\gtrsim 0.4M_{\odot}$), and low-mass ones ($\lesssim 0.25M_{\odot}$).

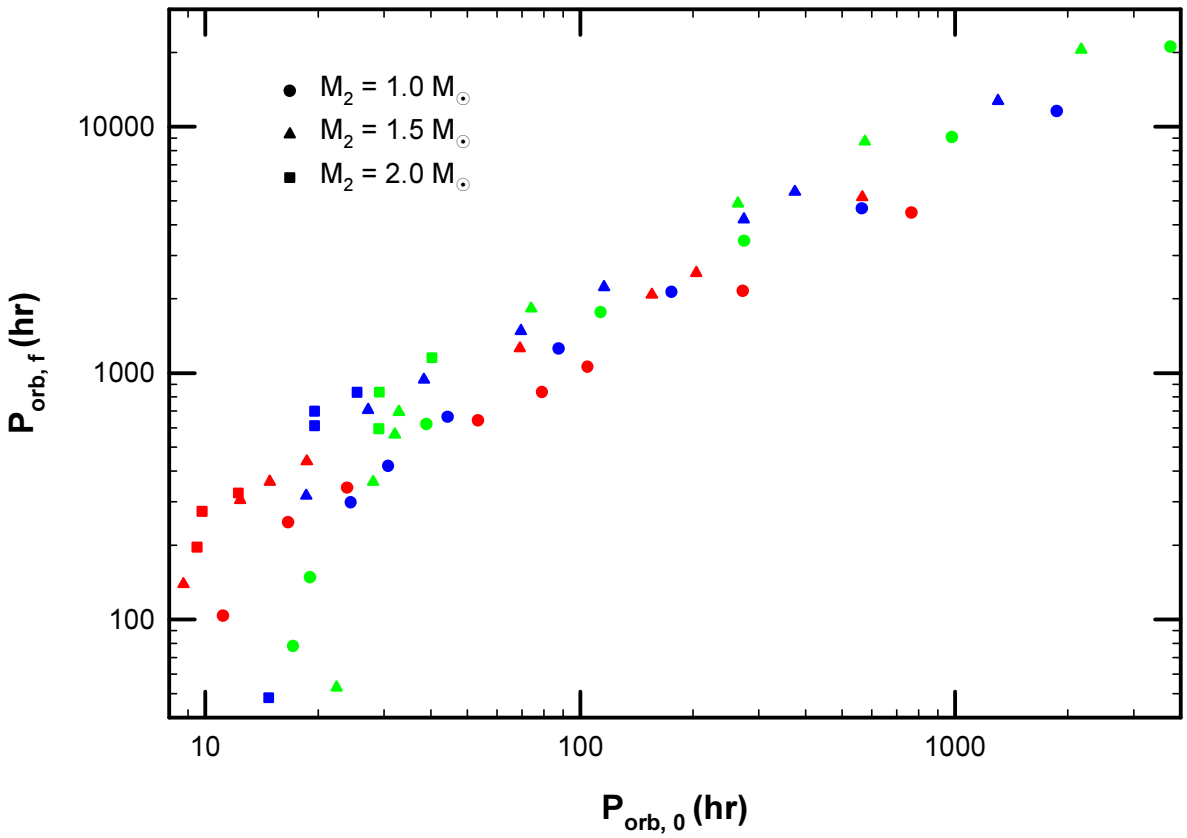

Fig. 22.— Dependence of the final orbital period ($P_{orb,f}$ in hours) on the initial orbital period ($P_{orb,o}$ in hours). The initial mass of the donors (at the onset of mass transfer) is denoted by circles, triangles, and squares as shown in the legend. The various shades of gray correspond to different metallicities (Z=0.02 is black, Z=0.004 is light gray, Z=0.0001 is medium gray). [In the electronic edition: The various colors correspond to different metallicities (Z=0.02 is green, Z=0.004 is blue, Z=0.0001 is red).] Although there is a strong linear dependence between the initial and final orbital periods for $P_{orb,o} \gtrsim$ 20hr, this relationship breaks down below this value (corresponding to systems with initial conditions that place them close to the bifurcation limit).

Table 1a. Representative Donor Properties[a] ($Z = 0.02$)

$(M_c/X_c)_o$	M_{2f}	t(Gyr)	$\log L$	$\log T_e$	$\log T_c$	$\log P_c$	X_c	$< X >$	$\log P_{orb,o}$	$\log P_{orb,f}$	M_{env}	$M_{X=0.1}$
$M_1 = 1.4M_\odot$, $M_{2o} = 1M_\odot$												
M_c=0.35	0.452	0.006	3.37	3.539	7.57	22.44	0.00	0.68	3.57	4.32	0.0082	0.0081
M_c=0.30	0.373	0.017	2.79	3.532	7.56	22.04	0.00	0.67	2.99	3.96	0.0104	0.0101
M_c=0.25	0.332	0.059	2.36	3.574	7.56	21.80	0.00	0.65	2.44	3.54	0.0096	0.0091
M_c=0.20	0.304	0.196	2.05	3.601	7.50	21.67	0.00	0.63	2.05	3.25	0.0088	0.0082
M_c=0.15	0.270	0.640	1.60	3.647	7.46	21.49	0.00	0.61	1.59	2.79	0.0088	0.0079
M_c=0.10	0.231	1.848	0.94	3.701	7.40	21.22	0.00	0.58	1.28	2.17	0.0119	0.0105
M_c=0.05	0.216	2.748	0.64	3.724	7.38	21.10	0.00	0.56	1.23	1.89	0.0136	0.0119
$M_1 = 1.4M_\odot$, $M_{2o} = 1.5M_\odot$												
M_c=0.30	0.377	<0.001	2.78	3.536	7.66	22.02	0.00	0.67	2.76	3.94	0.0096	0.0092
M_c=0.25	0.349	0.045	2.56	3.569	7.58	21.91	0.00	0.66	2.42	3.69	0.0079	0.0075
M_c=0.20	0.306	0.210	2.08	3.601	7.50	21.69	0.00	0.64	1.87	3.26	0.0082	0.0076
M_c=0.15	0.274	0.600	1.63	3.639	7.47	21.49	0.00	0.62	1.52	2.84	0.0092	0.0083
M_c=0.10	0.267	0.764	1.54	3.647	7.46	21.46	0.00	0.61	1.51	2.75	0.0095	0.0086
M_c=0.05	0.254	1.175	1.35	3.686	7.44	21.39	0.00	0.59	1.45	2.56	0.0087	0.0077
X_c=0.00	0.209	2.752	0.30	3.697	7.34	20.86	0.00	0.57	1.35	1.73	0.0341	0.0316
$M_1 = 1.4M_\odot$, $M_{2o} = 2M_\odot$												
M_c=0.10	0.299	0.172	1.87	3.620	7.62	21.53	0.00	0.61	1.60	3.06	0.0097	0.0088
M_c=0.00	0.285	0.297	1.73	3.633	7.57	21.48	0.00	0.60	1.46	2.92	0.0097	0.0089
X_c=0.10	0.274	0.548	1.58	3.651	7.55	21.41	0.00	0.58	1.46	2.77	0.0100	0.0089

[a]The properties of donors that evolve to become HeDD's at the point where they have just detached from their Roche lobes after evolving off the RGB.

Note. — The first column lists the values of either the central hydrogen content (X_c) or the helium core mass (M_c in solar masses) at the onset of mass transfer. M_{2f} is the (final) mass of the donor in units of $M_\odot$, and t (Gyr) denotes the age of the donor measured from the onset of mass transfer. $\log L$ is the log of the luminosity in solar units, and $\log T_e$ is the log of the effective temperature in Kelvin. Note that $\log T_c$ and $\log P_c$ are the logs of the central temperature (K) and central pressure (ergs/cm^2), respectively. X_c is the central hydrogen abundance and $< X >$ is hydrogen abundance averaged over the envelope of the donor. $\log(P_{orb,o})$ is the log of the initial orbital period (in hours) and $\log(P_{orb,f})$ is the log of the final orbital period (in hours). M_{env} is the mass of the H-rich envelope in units of $M_\odot$ and $M_{X=0.1}$ is the mass of the envelope measured from the surface to the point where the hydrogen mass fraction has decreased to 0.1. Note that 'na' is used wherever the results are Not Applicable.

Table 1b. Representative Donor Properties[a] ($Z = 0.004$)

$(M_c/X_c)_o$	M_{2f}	t(Gyr)	$\log L$	$\log T_e$	$\log T_c$	$\log P_c$	X_c	$< X >$	$\log P_{orb,o}$	$\log P_{orb,f}$	M_{env}	$M_{X=0.1}$
$M_1 = 1.4M_\odot$, $M_{2o} = 1M_\odot$												
M_c=0.35	0.435	0.007	3.18	3.582	7.66	22.33	0.00	0.67	3.27	4.06	0.0094	0.0092
M_c=0.30	0.378	0.020	2.73	3.614	7.65	22.03	0.00	0.65	2.75	3.67	0.0096	0.0092
M_c=0.25	0.335	0.075	2.32	3.632	7.56	21.81	0.00	0.64	2.24	3.33	0.0114	0.0107
M_c=0.20	0.311	0.200	2.07	3.651	7.51	21.69	0.00	0.63	1.94	3.10	0.0112	0.0104
M_c=0.15	0.291	0.381	1.78	3.681	7.51	21.55	0.00	0.62	1.65	2.82	0.0120	0.0109
M_c=0.10	0.276	0.618	1.56	3.693	7.50	21.44	0.00	0.61	1.49	2.62	0.0140	0.0127
M_c=0.05	0.265	0.870	1.39	3.705	7.49	21.36	0.00	0.63	1.39	2.47	0.0145	0.0138
$M_1 = 1.4M_\odot$, $M_{2o} = 1.5M_\odot$												
M_c=0.35	0.447	0.008	3.24	3.581	7.67	22.38	0.00	0.68	3.11	4.10	0.0096	0.0094
M_c=0.30	0.382	0.001	2.76	3.598	7.66	22.05	0.00	0.66	2.57	3.74	0.0092	0.0088
M_c=0.25	0.374	0.039	2.68	3.617	7.69	21.98	0.00	0.65	2.44	3.62	0.0097	0.0092
M_c=0.20	0.343	0.074	2.36	3.634	7.65	21.80	0.00	0.63	2.06	3.35	0.0108	0.0101
M_c=0.15	0.326	0.117	2.19	3.663	7.65	21.70	0.00	0.61	1.84	3.17	0.0098	0.0089
M_c=0.10	0.309	0.159	1.95	3.668	7.63	21.56	0.00	0.59	1.58	2.97	0.0131	0.0120
M_c=0.05	0.297	0.235	1.80	3.673	7.60	21.48	0.00	0.58	1.43	2.85	0.0157	0.0143
X_c=0.00	0.270	0.595	1.50	3.715	7.52	21.14	0.00	0.50	1.27	2.51	0.0346	0.0318
$M_1 = 1.4M_\odot$, $M_{2o} = 2M_\odot$												
M_c=0.10	0.292	0.056	1.90	3.673	7.71	21.20	0.00	0.37	1.40	2.92	0.0183	0.0212
M_c=0.00	0.279	0.117	1.78	3.672	7.63	20.89	0.00	0.40	1.29	2.85	0.0475	0.0425
X_c=0.10	0.272	0.340	1.72	3.681	7.60	21.16	0.00	0.38	1.29	2.79	0.0201	0.0170
X_c=0.30	0.214	2.743	0.73	3.819	7.43	20.45	0.00	0.22	1.17	1.68	0.0542	0.0444

[a]The properties of donors that evolve to become HeDD's at the point where they have just detached from their Roche lobes after evolving off the RGB.

Note. — See the *Note* beneath Table 1a for an explanation of all of the columns and symbols used in this table.

Table 1c. Representative Donor Properties[a] ($Z = 0.0001$)

$(M_c/X_c)_o$	M_{2f}	t(Gyr)	$\log L$	$\log T_e$	$\log T_c$	$\log P_c$	X_c	$< X >$	$\log P_{orb,o}$	$\log P_{orb,f}$	M_{env}	$M_{X=0.1}$
$M_1 = 1.4M_\odot$, $M_{2o} = 1M_\odot$												
M_c=0.35	0.445	0.013	2.98	3.670	7.66	22.36	0.00	0.65	2.88	3.65	0.0115	0.0109
M_c=0.30	0.395	0.038	2.57	3.684	7.65	22.09	0.00	0.64	2.43	3.33	0.0148	0.0139
M_c=0.25	0.357	0.129	2.21	3.703	7.57	21.89	0.00	0.63	2.02	3.02	0.0175	0.0162
M_c=0.20	0.349	0.168	2.08	3.706	7.60	21.81	0.00	0.63	1.90	2.92	0.0201	0.0186
M_c=0.15	0.330	0.250	1.95	3.716	7.60	21.63	0.00	0.54	1.73	2.81	0.0260	0.0237
M_c=0.10	0.307	0.354	1.65	3.739	7.58	21.41	0.00	0.50	1.38	2.53	0.0339	0.0307
M_c=0.05	0.297	0.467	1.49	3.747	7.57	21.29	0.00	0.48	1.22	2.39	0.0404	0.0362
X_c=0.00	0.272	1.170	1.09	3.776	7.52	20.98	0.00	0.41	1.05	2.02	0.0563	0.0493
$M_1 = 0.7M_\odot$, $M_{2o} = 1M_\odot$												
X_c=0.00	0.226	1.880	0.30	3.834	7.43	20.26	0.00	0.27	1.05	1.28	0.0961	0.0722
$M_1 = 1.4M_\odot$, $M_{2o} = 1.5M_\odot$												
M_c=0.35	0.459	0.014	3.06	3.666	7.67	22.42	0.00	0.66	2.75	3.71	0.0118	0.0113
M_c=0.30	0.405	0.041	2.67	3.681	7.66	22.15	0.00	0.64	2.31	3.41	0.0126	0.0118
M_c=0.25	0.394	0.058	2.56	3.686	7.68	22.07	0.00	0.63	2.19	3.32	0.0141	0.0131
M_c=0.20	0.350	0.078	2.29	3.699	7.66	21.73	0.00	0.48	1.84	3.10	0.0220	0.0199
M_c=0.15	0.318	0.114	1.80	3.735	7.65	21.30	0.00	0.40	1.27	2.64	0.0454	0.0407
M_c=0.10	0.312	0.142	1.73	3.747	7.63	21.24	0.00	0.39	1.17	2.56	0.0476	0.0425
M_c=0.05	0.307	0.218	1.66	3.756	7.61	21.21	0.00	0.38	1.11	2.48	0.0490	0.0435
X_c=0.00	0.283	0.897	1.25	3.771	7.55	21.02	0.00	0.40	0.94	2.15	0.0571	0.0508
$M_1 = 1.4M_\odot$, $M_{2o} = 2M_\odot$												
M_c=0.10	0.315	0.070	1.71	3.761	7.69	21.22	0.00	0.40	1.09	2.51	0.0466	0.0413
M_c=0.00	0.304	0.124	1.57	3.750	7.60	21.27	0.00	0.45	0.99	2.44	0.0435	0.0387
X_c=0.10	0.293	0.460	1.41	3.760	7.58	21.19	0.17	0.45	0.98	2.29	0.0468	0.0416

[a]The properties of donors that evolve to become HeDD's at the point where they have just detached from their Roche lobes after evolving off the RGB.

Note. — See the *Note* beneath Table 1a for an explanation of all of the columns and symbols used in this table.

Table 2a. Representative Donor Properties[a] ($Z = 0.02$)

$(M_c/X_c)_o$	M_{2f}	t(Gyr)	$\log L$	$\log T_e$	$\log T_c$	$\log P_c$	X_c	$< X >$	$\log P_{orb,o}$	$\log P_{orb,f}$	M_{env}	$M_{X=0.1}$
						$M_1 = 1.4M_\odot$, $M_{2o} = 1M_\odot$						
M_c=0.25	0.332	0.935	-1.50	4.214	7.36	22.09	0.00	0.27	2.44	3.54	0.0017	0.0011
M_c=0.20	0.304	1.128	-1.50	4.195	7.33	21.95	0.00	0.27	2.05	3.25	0.0021	0.0013
M_c=0.15	0.270	1.608	-1.50	4.171	7.30	21.75	0.00	0.29	1.59	2.79	0.0024	0.0017
M_c=0.10	0.231	3.024	-1.50	4.136	7.26	21.49	0.00	0.24	1.28	2.15	0.0039	0.0024
M_c=0.05	0.215	3.960	-1.50	4.126	7.26	21.36	0.00	0.22	1.23	1.85	0.0045	0.0029
X_c=0.00	0.251	0.985	-1.50	3.563	7.08	18.45	0.00	0.38	1.08	0.73	na	na
X_c=0.10	0.395	0.315	-1.50	3.541	7.00	17.40	0.10	0.56	0.98	0.70	na	na
X_c=0.20	0.420	0.259	-1.50	3.539	6.98	17.24	0.20	0.59	0.95	0.69	na	na
X_c=0.30	0.443	0.221	-1.50	3.536	6.96	16.87	0.30	0.62	0.93	0.69	na	na
						$M_1 = 0.7M_\odot$, $M_{2o} = 1M_\odot$						
X_c=0.00	0.251	0.443	-1.50	3.564	7.09	18.44	0.00	0.38	1.08	0.73	na	na
X_c=0.10	0.393	0.133	-1.50	3.540	7.00	17.37	0.10	0.56	0.98	0.69	na	na
X_c=0.20	0.415	0.106	-1.50	3.536	6.97	17.21	0.20	0.59	0.95	0.69	na	na
X_c=0.30	0.435	0.098	-1.50	3.533	6.95	17.08	0.30	0.62	0.93	0.69	na	na
						$M_1 = 1.4M_\odot$, $M_{2o} = 1.5M_\odot$						
M_c=0.25	0.349	0.874	-1.50	4.223	7.38	22.18	0.00	0.28	2.42	3.69	0.0014	0.0010
M_c=0.20	0.306	1.137	-1.50	4.197	7.33	21.96	0.00	0.27	1.87	3.26	0.0021	0.0013
M_c=0.15	0.274	1.536	-1.50	4.175	7.31	21.77	0.00	0.30	1.52	2.84	0.0023	0.0017
M_c=0.10	0.267	1.765	-1.50	4.170	7.30	21.73	0.00	0.28	1.51	2.75	0.0026	0.0018
M_c=0.05	0.254	2.246	-1.50	4.156	7.28	21.65	0.00	0.26	1.45	2.55	0.0031	0.0020
X_c=0.00	0.206	5.020	-1.50	4.093	7.21	21.30	0.00	0.23	1.35	1.59	0.0055	0.0031
X_c=0.10	0.194	1.684	-1.50	3.581	7.21	18.45	0.00	0.24	1.30	0.74	na	na
X_c=0.20	0.299	0.761	-1.50	3.550	7.12	17.60	0.13	0.42	1.28	0.74	na	na
X_c=0.30	0.357	0.546	-1.50	3.544	7.05	17.34	0.25	0.50	1.24	0.71	na	na
						$M_1 = 1.4M_\odot$, $M_{2o} = 2M_\odot$						
M_c=0.10	0.299	1.097	-1.50	4.194	7.35	21.91	0.00	0.28	1.60	3.06	0.0020	0.0014
M_c=0.00	0.285	1.262	-1.50	4.185	7.33	21.84	0.00	0.25	1.46	2.92	0.0024	0.0016
X_c=0.10	0.274	1.560	-1.50	4.176	7.31	21.77	0.00	0.24	1.46	2.77	0.0027	0.0018
X_c=0.30	0.249	1.080	-1.50	3.611	7.10	17.54	0.17	0.51	1.33	0.59	na	na

[a]Representative properties of donors/HeDD's that have evolved down to luminosities of $\log(L/L_\odot) = -1.5$.

Note. — See the *Note* beneath Table 1a for an explanation of all of the columns and symbols used in this table. The time $t(Gyr)$ is the age of the donor after its detachment from its Roche lobe (after it evolves off the RGB).

Table 2b. Representative Donor Properties[a] ($Z = 0.004$)

$(M_c/X_c)_o$	M_{2f}	t(Gyr)	$\log L$	$\log T_e$	$\log T_c$	$\log P_c$	X_c	$< X >$	$\log P_{orb,o}$	$\log P_{orb,f}$	M_{env}	$M_{X=0.1}$
$M_1 = 1.4M_\odot$, $M_{2o} = 1M_\odot$												
M_c=0.30	0.378	0.884	-1.50	4.249	7.37	22.33	0.00	0.19	2.75	3.67	0.0016	0.0009
M_c=0.25	0.335	1.013	-1.50	4.224	7.33	22.13	0.00	0.20	2.24	3.33	0.0023	0.0012
M_c=0.20	0.311	1.182	-1.50	4.210	7.31	22.01	0.00	0.20	1.94	3.10	0.0098	0.0088
M_c=0.15	0.291	1.414	-1.50	4.197	7.29	21.89	0.00	0.19	1.65	2.82	0.0033	0.0016
M_c=0.10	0.276	1.749	-1.50	4.184	7.27	21.80	0.00	0.19	1.49	2.61	0.0038	0.0018
M_c=0.05	0.265	1.976	-1.50	4.178	7.27	21.73	0.00	0.18	1.39	2.46	0.0041	0.0020
X_c=0.00	0.136	4.035	-1.50	3.712	7.16	19.17	0.00	0.14	1.18	0.42	na	na
X_c=0.10	0.283	0.767	-1.50	3.594	7.07	17.70	0.08	0.46	1.08	0.62	na	na
X_c=0.20	0.347	0.452	-1.50	3.581	6.99	17.37	0.18	0.56	1.02	0.61	na	na
X_c=0.30	0.368	0.371	-1.50	3.576	6.97	17.24	0.28	0.60	0.99	0.61	na	na
$M_1 = 0.7M_\odot$, $M_{2o} = 1M_\odot$												
X_c=0.00	0.179	0.947	-1.50	3.638	7.10	18.66	0.00	0.27	1.18	0.58	na	na
X_c=0.10	0.293	0.261	-1.50	3.591	7.06	17.62	0.12	0.47	1.08	0.61	na	na
X_c=0.20	0.346	0.156	-1.50	3.579	6.98	17.10	0.19	0.57	1.02	0.61	na	na
X_c=0.30	0.368	0.098	-1.50	3.575	6.96	17.21	0.30	0.60	0.99	0.61	na	na
$M_1 = 1.4M_\odot$, $M_{2o} = 1.5M_\odot$												
M_c=0.25	0.374	0.933	-1.50	4.246	7.37	22.31	0.00	0.19	2.44	3.62	0.0017	0.0009
M_c=0.20	0.343	1.038	-1.50	4.228	7.34	22.17	0.00	0.19	2.06	3.35	0.0023	0.0011
M_c=0.15	0.326	1.121	-1.50	4.219	7.32	22.08	0.00	0.18	1.84	3.17	0.0027	0.0013
M_c=0.10	0.309	1.155	-1.50	4.211	7.32	21.99	0.00	0.18	1.58	2.97	0.0029	0.0014
M_c=0.05	0.297	1.264	-1.50	4.203	7.31	21.92	0.00	0.18	1.43	2.85	0.0032	0.0015
X_c=0.00	0.270	1.601	-1.50	4.187	7.29	21.76	0.00	0.15	1.27	2.44	0.0040	0.0019
X_c=0.10	0.224	1.506	-1.50	3.632	7.10	17.66	0.13	0.30	1.14	0.55	na	na
X_c=0.20	0.293	0.839	-1.50	3.600	7.01	17.33	0.31	0.44	1.08	0.59	na	na
X_c=0.30	0.339	0.577	-1.50	3.587	6.97	17.19	0.42	0.53	1.03	0.60	na	na
$M_1 = 1.4M_\odot$, $M_{2o} = 2M_\odot$												
M_c=0.10	0.292	0.887	-1.50	4.207	7.34	21.87	0.00	0.11	1.40	2.92	0.0040	0.0017
M_c=0.00	0.279	1.059	-1.50	4.197	7.31	21.81	0.00	0.14	1.29	2.84	0.0039	0.0018
X_c=0.10	0.272	1.285	-1.50	4.192	7.30	21.76	0.00	0.13	1.29	2.78	0.0045	0.0019
X_c=0.30	0.214	3.623	-1.50	4.155	7.29	21.33	0.00	0.08	1.17	0.79	0.0083	0.0031

[a]Representative properties of donors/HeDD's that have evolved down to luminosities of $\log(L/L_\odot) = -1.5$.

Note. — See the *Note* beneath Table 1a for an explanation of all of the columns and symbols used in this table. The time $t(Gyr)$ is the age of the donor after its detachment from its Roche lobe (after it evolves off the RGB).

Table 2c. Representative Donor Properties[a] ($Z = 0.0001$)

$(M_c/X_c)_o$	M_{2f}	t(Gyr)	$\log L$	$\log T_e$	$\log T_c$	$\log P_c$	X_c	$< X >$	$\log P_{orb,o}$	$\log P_{orb,f}$	M_{env}	$M_{X=0.1}$
$M_1 = 1.4M_\odot$, $M_{2o} = 1M_\odot$												
M_c=0.35	0.445	0.792	-1.50	4.282	7.39	22.63	0.00	0.06	2.88	3.65	0.0018	0.0006
M_c=0.30	0.395	0.854	-1.50	4.261	7.36	22.42	0.00	0.09	2.43	3.33	0.0029	0.0008
M_c=0.25	0.357	0.992	-1.50	4.241	7.33	22.24	0.00	0.11	2.02	3.02	0.0035	0.0010
M_c=0.20	0.349	1.093	-1.50	4.236	7.32	22.21	0.00	0.11	1.90	2.92	0.0040	0.0011
M_c=0.15	0.330	1.156	-1.50	4.224	7.31	22.11	0.00	0.10	1.73	2.80	0.0048	0.0012
M_c=0.10	0.307	1.412	-1.50	4.212	7.28	21.99	0.00	0.09	1.38	2.52	0.0063	0.0014
M_c=0.05	0.297	1.569	-1.50	4.208	7.27	21.93	0.00	0.09	1.22	2.37	0.0070	0.0016
X_c=0.00	0.272	2.337	-1.50	4.189	7.25	21.78	0.00	0.08	1.05	1.81	0.0087	0.0018
X_c=0.10	0.252	0.740	-1.50	3.650	7.06	17.66	0.09	0.44	0.91	0.47	na	na
X_c=0.20	0.280	0.614	-1.50	3.642	7.02	17.47	0.17	0.51	0.89	0.48	na	na
X_c=0.30	0.308	0.469	-1.50	3.633	6.97	17.29	0.27	0.57	0.88	0.48	na	na
$M_1 = 0.7M_\odot$, $M_{2o} = 1M_\odot$												
X_c=0.10	0.238	0.357	-1.50	3.656	7.07	17.66	0.09	0.41	0.93	0.46	na	na
X_c=0.20	0.279	0.207	-1.50	3.639	7.00	17.41	0.19	0.52	0.89	0.47	na	na
X_c=0.30	0.301	0.144	-1.50	3.632	6.95	17.24	0.29	0.57	0.88	0.48	na	na
$M_1 = 1.4M_\odot$, $M_{2o} = 1.5M_\odot$												
M_c=0.35	0.459	0.803	-1.50	4.288	7.40	22.68	0.00	0.05	2.75	3.71	0.0016	0.0005
M_c=0.30	0.405	0.848	-1.50	4.265	7.37	22.46	0.00	0.09	2.31	3.40	0.0026	0.0007
M_c=0.25	0.394	0.905	-1.50	4.259	7.36	22.42	0.00	0.09	2.19	3.32	0.0029	0.0008
M_c=0.20	0.350	0.997	-1.50	4.236	7.32	22.21	0.00	0.10	1.84	3.10	0.0044	0.0011
M_c=0.15	0.318	1.009	-1.50	4.222	7.31	22.04	0.00	0.08	1.27	2.63	0.0060	0.0013
M_c=0.10	0.312	1.020	-1.50	4.219	7.31	22.01	0.00	0.07	1.17	2.55	0.0064	0.0014
M_c=0.05	0.307	1.134	-1.50	4.216	7.30	21.98	0.00	0.08	1.11	2.47	0.0066	0.0014
X_c=0.00	0.283	2.043	-1.50	4.198	7.27	21.84	0.00	0.08	0.94	1.97	0.0079	0.0017
X_c=0.10	0.207	1.344	-1.50	3.678	7.12	17.96	0.04	0.32	0.87	0.43	na	na
X_c=0.20	0.245	0.871	-1.50	3.658	7.06	17.62	0.13	0.41	0.85	0.45	na	na
X_c=0.30	0.277	0.799	-1.50	3.646	7.01	17.41	0.23	0.49	0.83	0.46	na	na
$M_1 = 1.4M_\odot$, $M_{2o} = 2M_\odot$												
M_c=0.10	0.315	0.983	-1.50	4.220	7.31	22.02	0.00	0.08	1.09	2.50	0.0062	0.0013
M_c=0.00	0.304	1.156	-1.50	4.213	7.28	21.97	0.00	0.08	0.99	2.42	0.0069	0.0015
X_c=0.10	0.293	1.562	-1.50	4.206	7.27	21.91	0.00	0.08	0.98	2.27	0.0075	0.0015
X_c=0.30	0.195	1.101	-1.50	3.709	7.09	17.69	0.10	0.25	0.90	0.35	na	na

[a]Representative properties of donors/HeDD's that have evolved down to luminosities of $\log(L/L_\odot) = -1.5$.

Note. — See the *Note* beneath Table 1a for an explanation of all of the columns and symbols used in this table. The time $t(Gyr)$ is the age of the donor after its detachment from its Roche lobe (after it evolves off the RGB).

Table 3a. Evolutionary Track[a] (Vigorous Shell Flash)

Point	Δt (Gyr)	$\log L/L_\odot$	$\log T_{eff}$(K)
1	7.44	1.33	4.596
2	7.82	0.54	4.521
3	13.15	-0.36	4.376
4	32.61	0.24	4.492
5	32.61	0.11	4.439
6	32.61	1.33	4.395
7	32.61	2.74	3.941
8	32.62	2.38	4.479
9	43.70	-0.73	4.326
10	196.8	-0.77	4.338

[a]Initial conditions correspond to $M_{2,o} = 1.5M_\odot$, $M_c = 0.10M_\odot$, and $Z = 0.004$.

Note. — Each Point is labeled in Figure 19. The explanation of the columns is the same as that given in the caption beneath Table 3a.

Table 3b. Evolutionary Track[a] (Mild Thermal Pulse)

Point	Δt (Myr)	$\log L/L_\odot$	$\log T_{eff}$(K)
1	0.80	2.70	4.328
2	1.18	2.05	4.805
3	1.21	1.00	4.686
4	1.23	0.60	4.618
5	1.62	0.00	4.505
6	4.52	-0.40	4.430
7	17.5	-0.60	4.394
8	127	-0.80	4.366
9	312	-1.00	4.337
10	1360	-1.75	4.195

[a]Initial conditions correspond to $M_{2,o} = 1.5M_\odot$, $M_c = 0.25M_\odot$, and $Z = 0.004$.

Note. — Each Point is labeled in Figure 18. Δt (in Gyr) is the age of the donor measured from the point when the donor detaches from its Roche lobe (just after evolving off the RGB). $\log L/L_\odot$ and $\log T_{eff}$(K) are the luminosities and effective temperatures of the donors at the respective points.